



UNIVERSITY OF TRENTO
INDUSTRIAL DEPARTMENT OF ENGINEERING
E-AGLE TRENTO RACING TEAM

~ . ~

ACADEMIC YEAR 2022-2023

Active Anti-roll Bar

Abstract

Active anti-roll bar is an electro-mechanical system mounted on vehicles, used to improve ride comfort during a corner. The purpose of this element is to reduce the roll effect due to the centrifugal force that is produced by a mass that it is accelerating during a round of a corner. This force tends to shift the mass of the car to the outside of the turn, causing the car to tilt. That is undesirable for car control, and a greater angle of roll causes a loss of time in reaction. The disadvantage of this element is that in order to keep more flat the vehicle the two suspensions of the car must be connected. This means that the effects of the bump on one wheel will be transferred to the other. To avoid this problem intervenes the active part, which permits to change the different responses of the system changing its stiffness. The purpose of this report is to develop the design of an active anti-roll bar that will be mounted on the car of the E-Agle Trento Racing Team. The idea is to develop an automatic control system that acts on the actuator to change the stiffness of the anti-roll bar based on the vehicle conditions. During the straights, it will be used in lower stiffness, while in the curves it will be at maximum stiffness. The system is based on two blades that will be attached to the suspensions in order to connect the two wheels. The deflections of these parts permit to absorb the bump given on a wheel and transform it into a force that keeps the other wheel attached to the road. The section of the blades is thought in order to have different stiffness of the structure with different orientations of them. This is possible by taking advantage of the different second moment of the area that the blades have with a different configuration. In order to change the orientation it is used an electric motor which is connected to the blades using a worm gear system.

Contents

1	Introduction	1
1.1	How Anti-Roll Bars Work	2
1.2	Bladed anti-roll bar	2
1.3	Report targets	3
1.4	Building constrains	4
2	Components	5
3	Blades	7
3.1	Concepts	7
3.2	Parameters	7
3.2.1	Internal analysis	8
3.3	Optimization	11
3.3.1	Decision matrix	11
3.3.2	Bearing Verification	12
4	Transmission	13
4.1	Motor-Blades	13
4.1.1	Concepts	13
4.1.2	Verification	13
4.2	Worm Gear support	14
4.2.1	Verification	15
4.3	Box-Body	16
4.3.1	Verification	16
4.3.2	Bearing Verification	17
5	Box	19
5.1	Parameters	19
5.2	Concepts	19
5.2.1	Decision matrix	20
5.3	Components	21
5.3.1	Verification	21
6	Motor	23
6.1	Motor	23
6.2	Transmission coupling	23
6.3	Motor support	23
6.4	Concepts	24
6.4.1	Decision matrix	24
6.5	Verification	25
7	Bolted Joints	27
7.1	General bolt verification procedure	27
7.1.1	Different type of load	27
7.1.2	Different type of verifications	29
7.2	Bolts of the box verification	30

CONTENTS

7.3	Bolts of the motor support verification	31
7.4	Bolts of the box-pin plate verification	32
Conclusions		35
Riferimenti		37
Elenco delle Figure		37
Indice		39
Technical Drawings		39

Chapter 1

Introduction

An anti-roll bar is a part of many suspensions systems that helps reduce the body roll of a vehicle during fast cornering or over road irregularities. It connects opposite (left/right) wheels together through short lever arms linked by a torsion spring. A anti-roll bar increases the suspension's roll stiffness (its resistance to roll in turns) independent of its spring rate in the vertical direction.

From the 1950s, production cars were more commonly fitted with anti-roll bars, especially those vehicles with softer coil spring suspension.



Figure 1.1: A consequence of the anti-roll bar removing

An anti-roll bar is intended to force each side of the vehicle to lower, or rise, to similar heights, to reduce the sideways tilting (roll) of the vehicle on curves, sharp corners, or large bumps. With the bar removed, a vehicle's wheels can tilt away by much larger distances, as shown in the figure 1.1.

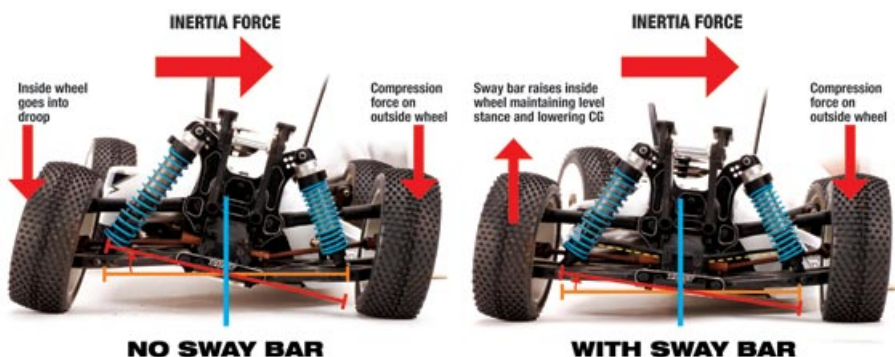


Figure 1.2: The inertia effect on the vehicle's suspensions during a turn, with or without an anti-roll bar

Although there are many variations in design, a common function is to force the opposite wheel's shock absorber, spring, or suspension rod to lower or rise to a similar level as the other wheel.

In a fast turn, a vehicle tends to drop closer onto the outer wheels, and the sway bar soon forces the opposite wheel to also get closer to the vehicle. As a result, the vehicle tends to "hug" the road closer in a fast turn, where all wheels are closer to the body. After the fast turn, the downward pressure is reduced, and the paired wheels can return to their normal height against the vehicle, kept at similar levels by the connecting sway bar (as it is shown in figure 1.2).

1.1 How Anti-Roll Bars Work

An anti-roll bars system is composed by three components all joined together: the main 'bar' is fixed to the body/chassis of the car with special mounts that allow it to rotate freely but hold it steady, and on each end there is a cantilever that attaches (often by links) to the rest of the suspension system.

This means the anti-roll bar is connected to both left- and right-side wheels, and its torsional properties act as a spring to resist body roll; when a car corners, weight is transferred to the outside wheel, which tries to rise up into the wheel arch. At the same time, the inside wheel wants to move out of the wheel arch. By connecting both sides together, an anti-roll bar resists this twisting motion and stops this from happening, transferring more load to the outside tyre to push the body back upright again, which in turn increases weight transfer. The stiffer the anti-roll bar, the more weight is transferred to the outside.

An anti-roll bar does very little when in a straight line, both left and right wheels are subject to the same bumps and undulations, and the anti-roll bar simply rotates in its mounts as the suspension is compressed and rebounded. But during cornering, the anti-roll bar is subjected to a twisting force, at which point it works together with the springs and dampers to control the car.



Figure 1.3: Adjustable roll-bar system, by changing the length of the cantilever

The amount of twisting force anti-roll bars resist and it's subjected to during cornering is often referred to as roll stiffness; a stiffer bar will resist the twisting action more than a softer one. Generally, this stiffness comes from the cross-sectional area (or thickness) of the bar.

Many of the aftermarket anti-roll bars available will offer a level of adjustment, usually by having multiple connecting points for the drop links, as you can see in the figure 1.3. These series of holes effectively alter the length of the cantilever and therefore alter the stiffness of the anti-roll bar; the longer the cantilever, the less effort is required to move it, or the softer the setting. The shorter the cantilever, the stiffer the setting.

Some motorsport applications make use of a different design, known as bladed anti-roll bars, which offer much more adjustment and levels of fine-tuning.

1.2 Bladed anti-roll bar

The bladed anti-roll bar is a type of adjustable anti-roll bar that permits one to change his behaviour instead of its orientation. This particular mechanism is composed of three main components: the main 'bar' that is fixed to the car's chassis that can rotate freely and, on each end, are mounted two blades (figure 1.4).

The way the blade works is that they are the stiffest in the vertical position and gradually get softer as they flatten out. In fact, the blade when flat has less inertia, so with a lower force can flex without transmitting torque to the main bar. When the blades are vertical instead, their moment of inertia

increases a lot, up to being stiffer than the main bar and therefore transmitting all the twisting moment to it. In case the main bar is perfectly rigid, the connection between the two wheels is perfectly rigid too, consequently, the suspensions don't work.

By rotating the blades then, the vehicle behaviour during cornering and on a straight line changes. In the first case, the ideal behaviour is to have a perfect rigid connection between wheels and the vehicle's body so as to avoid body roll and have a better steering response. On a straight line instead, the vehicle's suspensions should work individually, so as to be able to absorb the roughness of the terrain without modifying the behavior of the wheel on the opposite side.

To have good behavior in both situations with this type of manual anti-roll bar a trade-off is necessary. For this reason, in some sport vehicles, are used systems that permit to change the anti-roll bar behaviour while driving without having to stop and do it manually. Those systems are called active anti-roll bars.

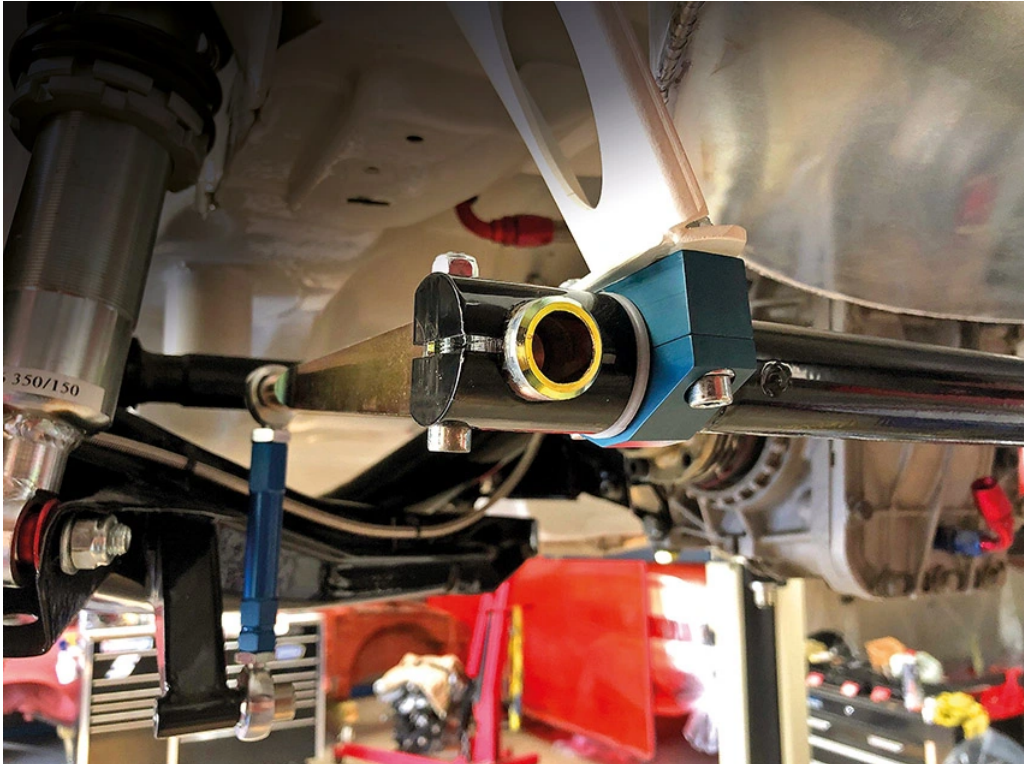


Figure 1.4: Bladed anti-roll bar

1.3 Report targets

In this report it is presented a system of an active roll-bar for a Formula SAE vehicle. The main goals that we have to achieve are:

- Building an active anti-roll bar starting from the previous one (a manual-bladed anti-roll bar);
- Optimize the blades' shape in order to have the best response in their main two configurations (softer and stiffer one);
- Verify (failure, fatigue, bending, etc) all the mechanism's components;
- Minimize the system's overall dimensions and so its total final weight;
- Respect the building constraints.

1.4 Building constrains

The mechanism will be mounted between the rear suspension system. In order to avoid collision between the active anti-roll bar, the suspension or the car body, the overall dimensions must be inside some limits as can be seen in figure 1.5. The overall dimensions are:

- Maximum height (h): 100 mm
- Maximum width (w): 108 mm
- Maximum length (l): 50 mm

As regards the blades instead, analyzing the structure of the suspensions and the forces acting on the wheels, the studies carried out previously were confirmed which found the maximum forces acting on the blades equal to $F = 591kN$. This force is transmitted to the blades through two bars connected to the suspensions on each side. For having the force acting always in the shear centre, the connection between the elements is done with UNIBALL bearings.



Figure 1.5: Maximum overall dimensions of the active anti-roll bar

All the project specifications are summed up in the table 1.6.

Specification	Weight	Target Value	R/D
Weight	5	0,5 Kg	R
Size a (Depth)	5	50 mm	R
Size c (Height)	5	100 mm	R
Size b (Width)	20	108 mm	R
Fatigue Life	4	10^4	D
Max stiffness	5	max	D
Min stiffness	5	min	D
Max roll angle at 2g	6	2°	R
Min Deflection	4	2 mm	D
Max deflection	5	10 mm	D
Number of parts	2	min	D
Actuation time from min to max stiff	4	0,3 s	R
Max Force in duty	5	1,2 kN	R
Torque motor	6	min	D
Lenght of flexure	6	100 mm	R
Sigma max(Material)	7	1200 Mpa	R
Elastic Module Material	6	min	D

Figure 1.6: Table of specifications

Chapter 2

Components

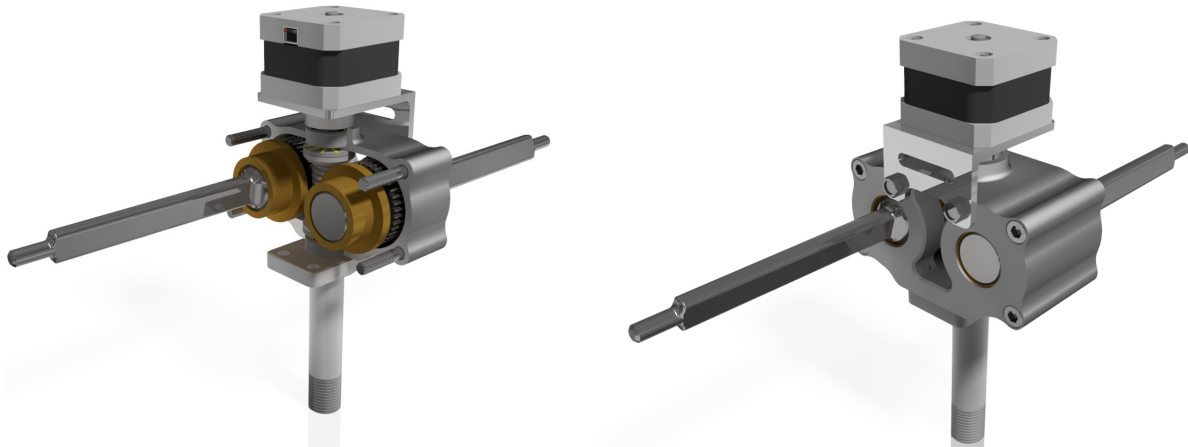


Figure 2.1: Final concept of the total system of active anti-roll bar

As the active anti-roll bar is a complex system, the process of designing the system was made by dividing the mechanism into its main components and then studying them one by one. The main subsystems that we identified are:

1. Blades: bending, cross-section area, length;
2. Transmission: blades rotation, box rotation, etc;
3. Box: shape, weight, resistance;
4. Motor: optimal motor, motor-transmission coupling, mounting.

For each component are specified the parameters and characteristics that it must have, this is to then generate at least two concepts, to then select the most suitable one, comparing it to our decision matrix. Once the concept is chosen, it must be verified with the forces and moments applied to it.

For each component, there is therefore a broad discussion, for this reason, a chapter has been dedicated to each subsystem

Chapter 3

Blades

3.1 Concepts

The blades are the main component of the anti-roll bar, for this reason have been explored a large number of solutions to really choose the best option, this includes the material type, shape and dimensions.

The materials that are the most suitable are music wire steel, titanium and aluminium; for what concerns the cross-sections the rectangular and elliptical, then two different shapes of the blades are considered.

This last choice deserves two more lines. The first idea was in fact to use a cross-section with a certain shrinkage from the base of the blade to the tip (where the force is applied). This can be seen on one hand as an attempt of using the material more efficiently and, on the other hand, to have a bending of the blades as uniform as possible, along the full length.

3.2 Parameters

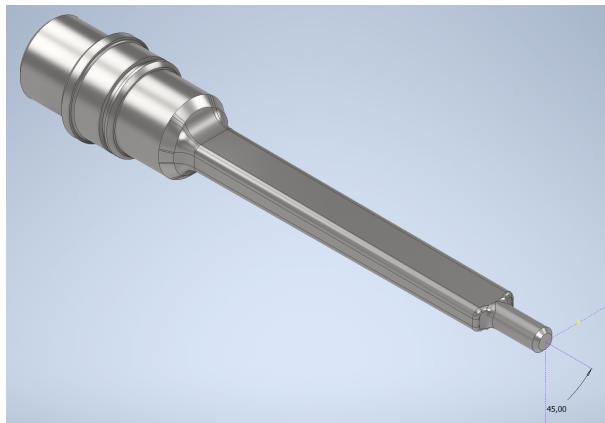


Figure 3.1: Blades' model

The first part of the analytical analysis is made by creating a blade model. From the drawing we fixed the length L , the width b_0 and the height h_0 . Another important aspect consists in defining the forces applied on the blades, this can be done by applying a load at the rear of the car and measuring the compression of the spring, then knowing the elastic coefficient of the spring, can be calculated the force using the Young equation ($F = k_m x_m$). The measured compression (x_m) is equal to 12mm that has been incremented to 15mm giving a safety factor of 1.25.

Furthermore, other important parameters are the inter-axle spacing between the two journal bearings p and the distance between the base of the blade and the inter-axle spacing of the second journal bearing q . Now all the parameters are listed in the following table, where s and dc are respectively the bearings' thickness and diameter.

PARAMETERS	VALUES	PARAMETERS	VALUES
L	100 mm	p	28.4 mm
q	13.45 mm	s	7 mm
dc	20 mm	k_m	39.4 N/mm
x_m	15 mm	F	591 N

Considering the maximum force, it's possible to size the uniball attached at the extreme of the blade. From the catalogues, taking into account that h is fixed, b can be no less than 6mm. So in the tapered case, the maximum inclination is easily calculated as

$$k_{max} = \frac{b_0 - 6}{L}. \quad (3.1)$$

3.2.1 Internal analysis

From a static point of view, the blade can be represented by a beam connected by two hinges (the two journal bearings) to the box, which represents the frame.

Having defined the constraints and forces, it can be performed the actual static analysis of the blades.

So initially the rectangular section has an area that is easily calculated by the product between the height and the width of the blade. For our concept is very important that the stiffness in two perpendicular directions are very different. Considering an element in rotation, the moment of inertia is also subjected to variations in value.

Instead of rotating the blade and so changing the inertia in x and y directions, it can be rotated the force itself, this simplified the computation while obtaining the same solution. So the inertia of the bearing according to our reference frame is:

$$I_c = \frac{\pi \cdot dc^4}{64}; \quad (3.2)$$

and for the blades with rectangular section is:

$$I_y = \frac{h^3 \cdot b}{12}; \quad (3.3)$$

$$I_x = \frac{b^3 \cdot h}{12}.$$

While, considering for the elliptic section the major axis h and minor b, the moment of inertia is:

$$I_y = \pi \cdot \frac{\frac{h^3}{2} \cdot b}{8}; \quad (3.4)$$

$$I_x = \pi \cdot \frac{\frac{b^3}{2} \cdot h}{8}.$$

Static analysis

As all the parameters are defined, the mechanical stress analysis of the blades can be performed. By the free body diagram the results are:

$$Ra = F \cdot \frac{L + q}{p}; \quad (3.5)$$

$$Ra = F \cdot \frac{L + p + q}{p}.$$

As regards the moment applied:

$$\begin{cases} Mx = -Fy \cdot \frac{z \cdot (L+q)}{p} & \text{for } 0 \leq z \leq p \\ My = Fx \cdot \frac{z \cdot (L+q)}{p} & \text{for } p \leq z \leq p + q + L \end{cases} \quad (3.6)$$

The figures below show the actions applied in the X and Y directions.

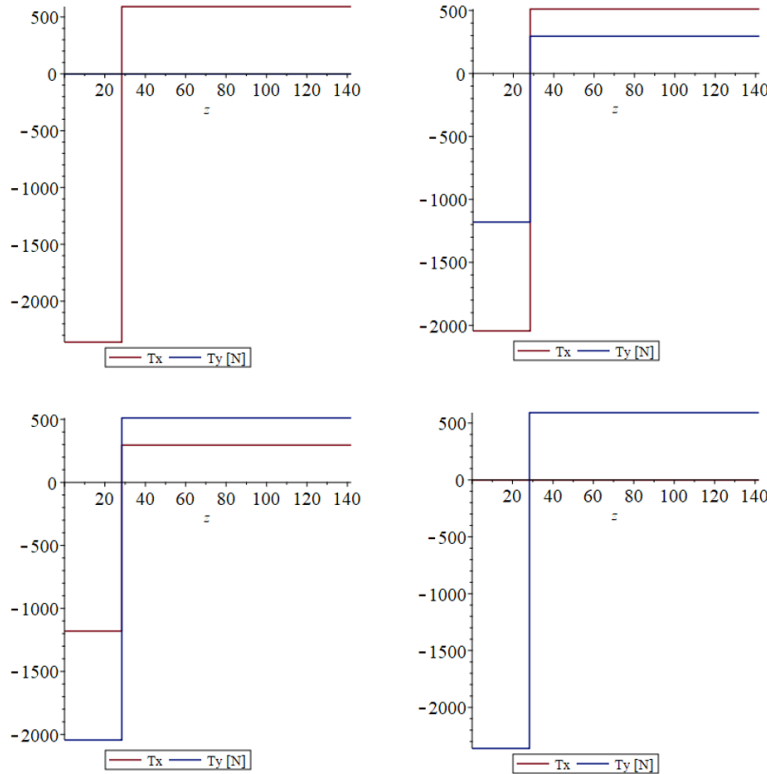


Figure 3.2: Internal forces applied on the blade for different angles of rotation

Then the moment applied are the following. Such as in the previous graphs the angle of rotation of the blades is between zero and $\frac{\pi}{2}$. The two intermediate results are for $\theta = \frac{\pi}{6}$ and $\theta = \frac{\pi}{3}$.

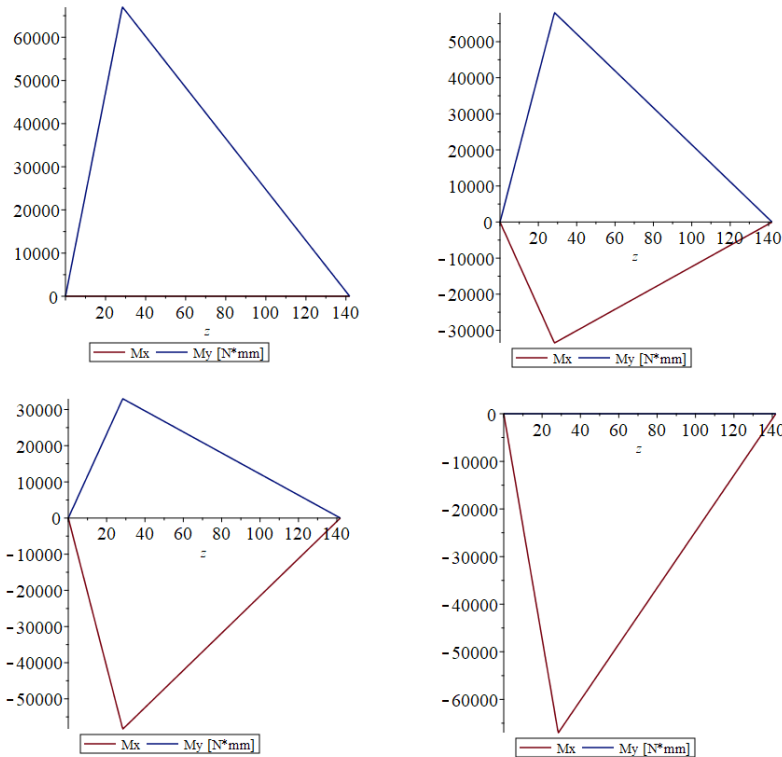


Figure 3.3: Moments applied on the blade for different angles of rotation

Because the section is not regular in the whole blade, also the internal stress changes along the length the σ is:

$$\begin{cases} \frac{Mx \cdot dc}{2 \cdot I_x} - \frac{My \cdot h}{2 \cdot I_c} & \text{for } 0 \leq z \leq p \\ \frac{Mx \cdot b}{2 \cdot I_x} - \frac{My \cdot h}{2 \cdot I_y} & \text{for } p \leq z \leq p + q + L \end{cases} \quad (3.7)$$

So the results are:

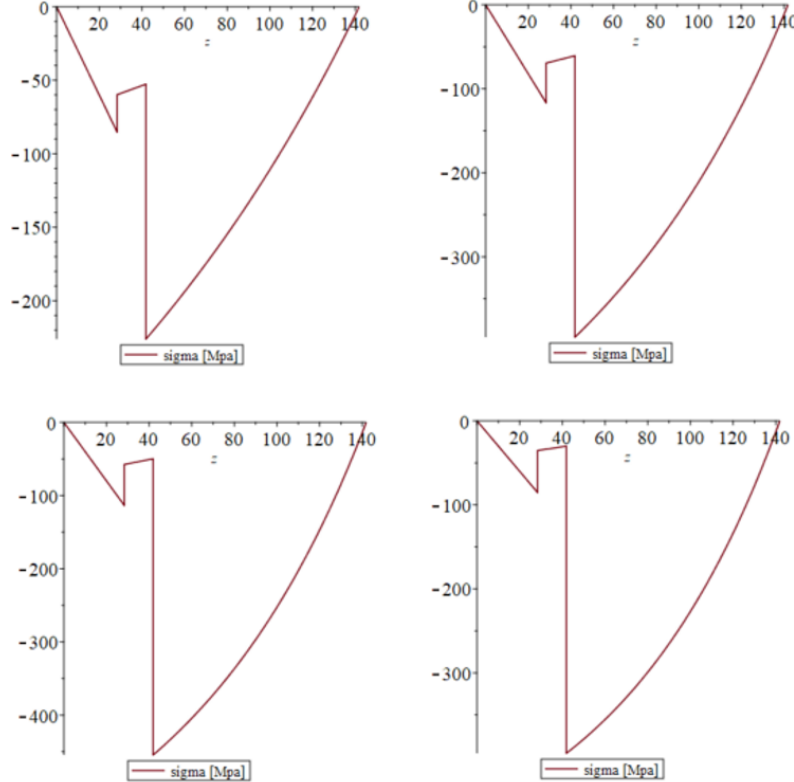


Figure 3.4: Internal stress of the blade for different angles of rotation

Sigma could be also shown in a 3D plot where in the axis there are the inclination and the distance from the origin of the base of the blade.

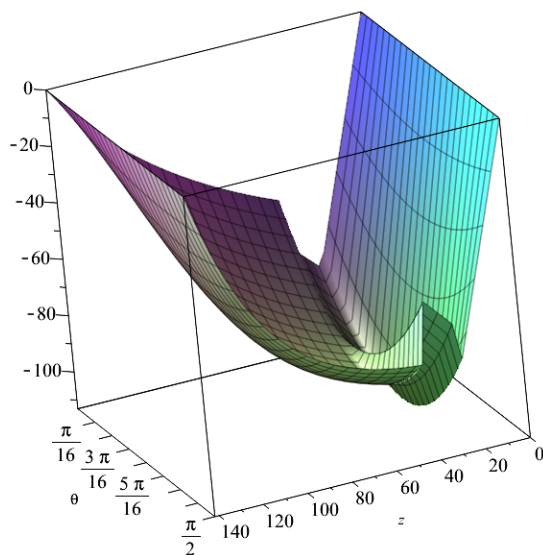


Figure 3.5: Internal stress of the blade in 3D. $b_0=15$, $h_0=20$, $k=0.07$.

3.3 Optimization

One of the most important characteristics of this active anti-roll bar is, as it's already said, the bending and not torsional behavior. So it's massively relevant obtaining the deformation of the blades. In order to do it has been used Castigliano's theorem. So the derivative of the energy compared to every force applied:

$$\frac{\partial U_x}{\partial F_i} = \int_L \frac{My}{EIy} \cdot \frac{\partial My}{\partial Fx} dz = \int_0^p \frac{Fx(z^2(L+q)^2)}{EIy \cdot p^2} dz + \int_p^{L+p+q} \frac{Fx(L+p+q-z)^2}{EIy} dz; \quad (3.8)$$

$$\frac{\partial U_y}{\partial F_i} = \int_L \frac{Mx}{EIx} \cdot \frac{\partial Mx}{\partial Fy} dz = \int_0^p \frac{Fy(z^2(L+q)^2)}{EIx \cdot p^2} dz + \int_p^{L+p+q} \frac{Fy(-L-p-q+z)^2}{EIy} dz.$$

So given the distribution of the sigma along the blade, the function to minimize has been defined. In particular, the aim is to distribute uniformly the stress all over the element to take full advantage of the material. In this sense, the derivative is minimized. Then is important to maximize the displacement between the position with maximum and minimum inertia, so with a rotation of 0 and 90 degrees.

The results are different for different cross-sections and materials. To analyze what is the best option it has been collected all the results in the decision matrix are shown in the next section.

3.3.1 Decision matrix

To choose the best solution for the production of the blades it has been used the decision matrix.

Every concept has a grade for each of the following specifications:

- Weight of the blade;
- Difficulty of manufacturing the blade;
- The maximum displacement of the blades at the point of application of the force;
- The difference between the maximum displacement and the minimum displacement;
- The safety factor of the blade relates to the yielding stress of the material;

			Rectangular cross section																				
			k equal to zero						k different to zero														
			Aluminium			Music wire steel			Titanium			Aluminium			Music wire steel			Titanium					
Specifications	Weight	Parameter	Mag	Score	Value	Mag	Score	Value	Mag	Score	Value	Mag	Score	Value	Mag	Score	Value						
Weight	0,05 g	Great	10	0,5		Fair	4	0,2	Good	8	0,4	Great	10	0,5									
Easy to manufacture	0,1 Ranking	Good	8	0,8		Great	10	1	Fair	4	0,4	Good	8	0,8									
Max Displacement	0,28 mm	4,7	3	0,825		5,2	4	1,1	8,7	10	2,75	6,1	5,5	1,5125									
Delta of Displacement	0,4 mm	2,9	3	1,2		3,3	4	1,6	6	10	4	4,2	6	2,4									
Safety Factor	0,18 %	1,13	0	0		0	1,12	0	0	1,2	2	0,35	1,14	0,5	0,0875								
			Overall Value			3,325			3,9			7,9			5,3								
			Elliptic cross section																				
			k equal to zero						k different to zero														
			Aluminium			Music wire steel			Titanium			Aluminium			Music wire steel			Titanium					
Specifications	Weight	Parameter	Mag	Score	Value	Mag	Score	Value	Mag	Score	Value	Mag	Score	Value	Mag	Score	Value						
Weight	0,05 g	Great	10	0,5		Fair	4	0,2	Good	8	0,4	Great	10	0,5									
Easy to manufacture	0,1 Ranking	Good	8	0,8		Great	10	1	Fair	4	0,4	Good	8	0,4									
Max Displacement	0,28 mm	3,4	1	0,275		2,7	0	0	4,9	3,5	0,9625	5,2	4	1,1	3,4	1	0,275	6,2	5,5	1,5125			
Delta of Displacement	0,4 mm	1,9	0,5	0,2		1,7	0	0	3,1	3,5	1,4	3,6	4,5	1,8	2	2	0,8	4,3	6	2,4			
Safety Factor	0,18 %	1,14	0,5	0,0875		1,43	7	1,225	1,56	10	1,75	1,27	3,5	0,6125	1,43	7	1,225	1,56	10	1,75			
			Overall Value			1,8625			2,49			4,8125			5,5			6,46					

Figure 3.6: Blades decision matrix, for the shape choice

From the analysis of the decision matrix (figure 3.6), the configuration with the shrinkage was possible and effective only with the aluminium material. This is due to the high-yielding strength of both steel and titanium that permit to have a very tiny cross-section without lowering a lot the safety factor of the structure.

The elliptic cross-section was indeed not very effective concerning the simpler-to-manufacture rectangular cross-section.

3.3.2 Bearing Verification

Having the reacting forces, it is possible to choose the model of the bearings. The load on these supports is pretty high and the space on the box is limited. For this reason, it has been chosen Solid bronze flanged bushing, which allows high load with very thin thickness with respect to comparable ball bearings.

The bearings need to support, in the worst case, 2951 N.

From the SKF catalogue, it is found the following model: PBMF 202615M1G.

Dimensions		Properties	
Bore diameter	20 mm	Design	Flanged
Flange diameter	35 mm	Material	Solid bronze
Flange thickness	4 mm	Relubrication feature	With
Outside diameter	26 mm		
Width	15 mm		

Figure 3.7: Data Sheet of SKF PBMF 202615M1G

As shown in 3.7, the static allowable load is 15.6 KN which is 4.6 times larger than the max force on it, and as in the system the load is mainly static because the blades have only $\pm 90^\circ$ of rotation, so the bushings are verified.

Chapter 4

Transmission

4.1 Motor-Blades

To actuate the system it is necessary to design a transmission between the blades and the motor. As the forces applied to the tip of the blades are not in the horizontal plane, to have the same variation of the moment of inertia per unit angle, it is necessary to rotate the two blades in opposite directions. Having this constraint allowed us to generate two concepts:

4.1.1 Concepts

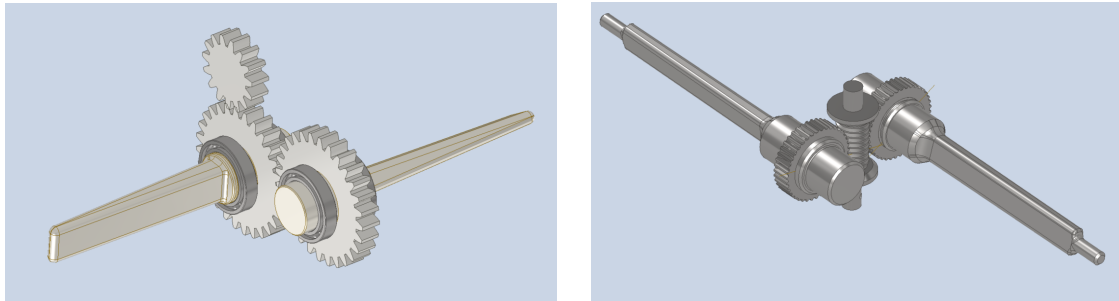


Figure 4.1: a) First concept b) Second concept

In the first concept, as shown in figure 4.1 a, we used three gears, the one on top is needed to connect the motor to one of the two blades, and the second one is driven from the first. This is a simple design, but the downside is that it is asymmetric which causes the first blade to have higher stresses, caused by both being actuated and actuating. The other issue is that the mechanism is reversible, so every torque coming from the blades, will act on the motor. This last point is really important as it is one of the specifications in the QFD. Then the most limiting factor of this design is the dimension of the assembly as it exceeds the one specified in the specification.

The second design takes into account all the issues above. As shown in figure 4.1 b, the choice of using a worm gear has many advantages. First of all the mechanism is irreversible so for any torque on the blade, there is no torque on the motor. Then using this system it is possible to obtain a high transmission ratio, and this aspect is quite important because it allows precise positioning of the blade, while the rotating speed is not so important. Another advantage is the dimension, while the first concept has a wheelbase of 63mm between the two blades, the second one has just 44mm, which is a space reduction of 30 %. Thanks to all his advantages, the chosen concept is the one of the worm gear concept.

The connection to the motor is shown in detail at 6.3.

4.1.2 Verification

After choosing the concept, it is necessary to verify each component. Starting from the two gears and the worm gear: the torque involved is very low, and the main specification is the wheelbase that must be

minimized to reduce the space required, but having an internal diameter that allows mounting it to the blade.

The chosen gears and worm gear are from the KHK catalogue.



Figure 4.2: Data sheet of worm gear

It has been chosen a couple of worm gear and gear in order to have a large transmission ratio and at the same time a small wheelbase. The KWG0.8-R1 worm gear and AG0.8-40R1 respects this characteristic. For both of the models, the dimensions of the shaft (of the worm gear) and the internal radius (of the two gears) are not right, so one option is to home-make the custom gears with the same characteristics but with the right dimensions, or buying the KHK ones and then modify afterwards the dimensions. The second option is the preferred one, considering especially the costs involved. The final dimension of the component is shown in the technical drawing.

Total length	Web thickness	Web O.D.	Mounting distance	Allowable torque (N·m) <small>NOTE 1</small>								Backlash (mm)	Weight (kg)	Catalog Number
				J	30 rpm	100 rpm	300 rpm	600 rpm	900 rpm	1200 rpm	1800 rpm			
12	—	—	—	9.5	0.52	0.44	0.36	0.30	0.26	0.24	0.21	0.02~0.14	0.0056	AG0.5-20R1
				9.5	0.51	0.42	0.33	0.27	0.24	0.22	0.19		0.0056	AG0.5-20R2
				12	1.09	0.94	0.77	0.65	0.58	0.53	0.48		0.012	AG0.5-30R1
				12	1.09	0.92	0.73	0.60	0.54	0.49	0.43		0.012	AG0.5-30R2
				14.5	1.86	1.60	1.34	1.15	1.02	0.94	0.84		0.020	AG0.5-40R1
				17	2.82	2.42	2.05	1.77	1.58	1.46	1.30		0.035	AG0.5-50R1
16	—	—	—	19.5	3.94	3.41	2.89	2.50	2.26	2.08	1.87		0.053	AG0.5-60R1
				14	1.78	1.50	1.21	1.00	0.88	0.82	0.71	0.06~0.17	0.018	AG0.8-20R1
				14	1.76	1.44	1.11	0.91	0.80	0.74	0.63		0.018	AG0.8-20R2
				18	3.77	3.21	2.62	2.20	1.96	1.81	1.61		0.043	AG0.8-30R1
				18	3.75	3.14	2.46	2.02	1.80	1.65	1.45		0.043	AG0.8-30R2
				22	6.45	5.49	4.55	3.87	3.46	3.19	2.83		0.068	AG0.8-40R1
				26	9.75	8.31	6.94	5.94	5.34	4.96	4.38		0.10	AG0.8-50R1
				30	13.6	11.7	9.77	8.39	7.63	7.05	6.27		0.14	AG0.8-60R1

Figure 4.3: Data Sheet of allowable Load on worm gear

KHK provides also the allowable load 4.3. The current system has a maximum torque provided by the motor of 0.55Nm, which is much smaller than the maximum torque allowable.

4.2 Worm Gear support

The worm gear is used to transmit the torque generated by the motor to the blades, which are positioned on an axis that is orthogonal to the worm gear. This causes the generation of axial forces, which change direction each time there is an inversion of the motion. In order to support this load are needed Needle roller thrust bearings (as represented in figure 4.4). This solution has been chosen because of their little space in the axial direction and for the high relative load support related to their dimensions.

The worm gear should be supported also in the radial direction, to permit rotation. This is done by ball bearings, as represented in figure 4.4.

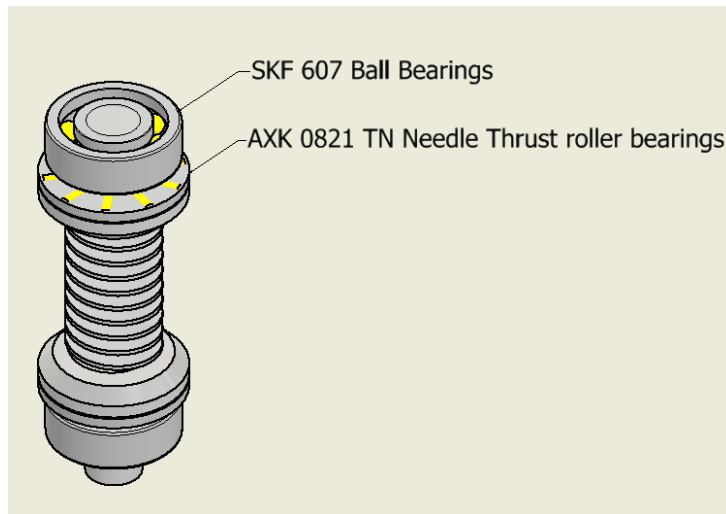


Figure 4.4: Bearings used to support the worm gear

The models of the two types of bearings are taken from the SKF catalogue. The selection is mostly based on their dimension because the space available was very little. After choosing the types that verify the constraints, is checked that they can carry the loads applied.

In order to fix the position of the bearings, the worm gear has been modified to obtain a flat surface where the bearings can transmit the force from the gear to the chassis.

4.2.1 Verification

To verify the thrust bearings first is needed to have the parameters of the worm gear, provided from the catalogue of KWG. Then it is possible to calculate the axial force on the worm gear using the relation:

$$F_x = \frac{F t_1 (\cos(\alpha) \cos(\lambda) - \mu \sin(\lambda))}{\cos(\alpha) \sin(\lambda) + \mu \cos(\lambda)} = 695N$$

Where:

- $F_{t1} = \frac{2000T}{d_1}$ is the force needed to apply the max torque T of the electric motor.
 - $T = 0.5 \text{ Nm}$ Max electric motor torque;
 - $\alpha = 20^\circ$ Pressure angle;
 - $\lambda = 3.8^\circ$ Lead Angle;
 - $\mu = 0.05$ Friction coefficient;

This force has to be contrasted by the thrust bearings, that has an allowable force equal to 20 kN in static conditions (as can be seen in figure 4.5).

Dimensions	Performance	
Bore diameter	8 mm	7.2 kN
Outside diameter	21 mm	20 kN
Thickness	2 mm	11 000 r/min
	Reference speed	5 600 r/min

Figure 4.5: Data Sheet of SKF AXK 0821 TN

The ball bearings are not needed to verify thanks to the symmetry of the system. The only thing that they have to do is to permit the rotation of the worm gear.

4.3 Box-Body

To connect the box of the active Anti-Roll Bar to the chassis of the car the solution that has been chosen is a simple pin bolted to the box. The other solution that was taken into account was to make a thru-axle with the worm gear integrated. This last option was impossible to integrate into our systems because the forces applied to the worm gear were too high.

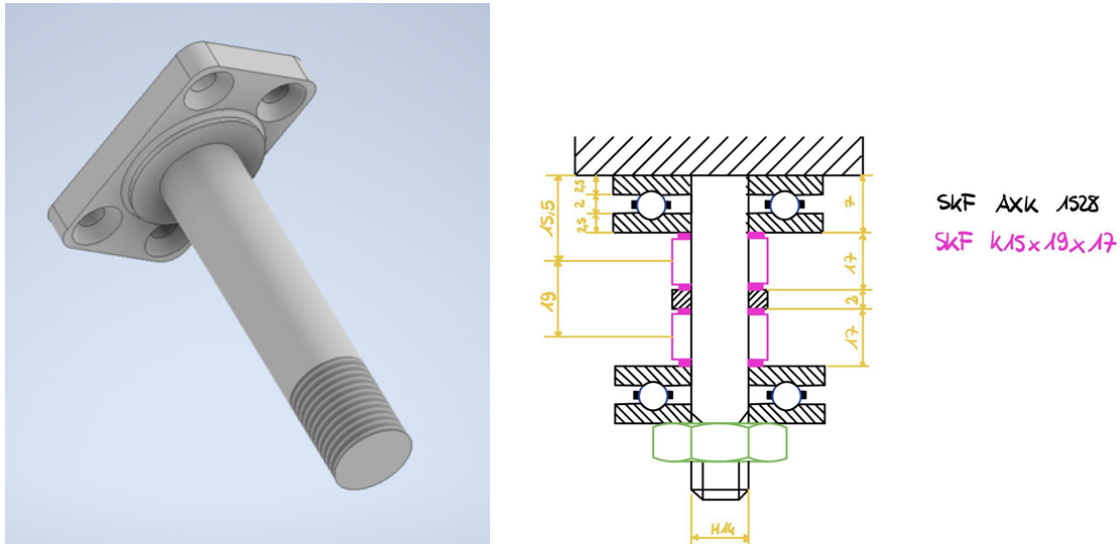


Figure 4.6: 3d Model and scheme of the pin

4.3.1 Verification

To perform the verification we assume the pin to be a beam connected by two hinges to the support on the car's chassis. The hinges are the two axial bearings that permit the structure to rotate. The effect on rigidity and stress of the roller bearings are in this case neglected.

The forces are the ones applied at the end of the blades as shown on 4.7 where is shown also the free body diagram of the pin.

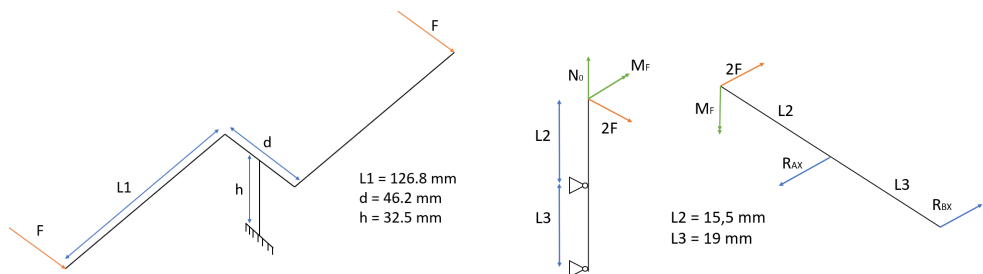


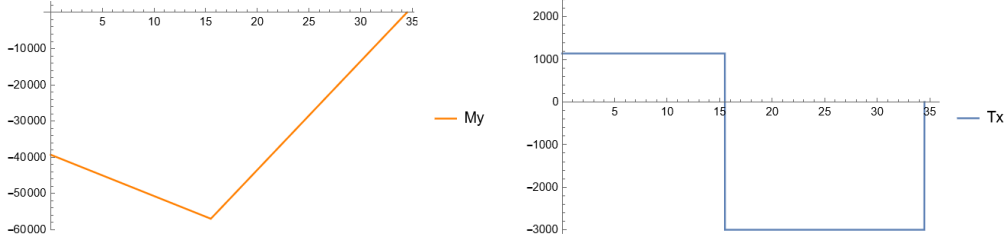
Figure 4.7: Model of the pin

The equations that result from the analysis of the free body diagram are:

$$\begin{cases} R_{ax} = 2F + R_{bx}; \\ M_F - L_3 R_{ax} = -2F(L_2 + L_3); \end{cases}$$

The next step is to solve the equilibrium equations to calculate the reactions acting on the bearings; these results being respectively $4.14kN$ for the bearing near the box(R_{ax}) and $3.0kN$ for the one far away(R_{bx}).

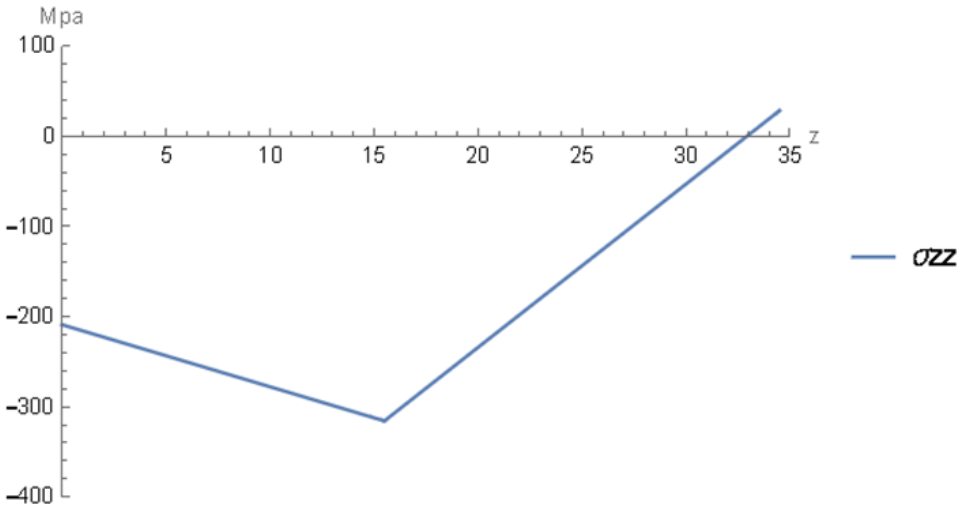
Then it can be computed and then plotted the internal forces acting on the pin, in this case, the bending moment M_y and the shear force T_x .


 Figure 4.8: Plot of M_y and T_x

After the plots of M_x and T_x , it can be plotted the function of σ_{zz} along the length of the pin to find the point at which the stress is the highest. To compute the stress we used the following formula:

$$\sigma_{zz}(z) = \frac{My(z) \cdot d}{I_{xx}}.$$

Where d is the diameter of the pin, equal to 15mm , and $I_{xx} = \pi \frac{d^4}{64}$.


 Figure 4.9: Plot of σ_{zz}

At this point is immediate to see that the maximum σ_{zz} is equal to -315.8MPa in correspondence with the bearing nearer to the box. The same thing happens with the shear stress, which has a maximum value of 22.6MPa .

The equivalent Von Mises stress can be computed with the following formula:

$$\sigma_{eq} = \sqrt{\sigma_{max}^2 + 3\tau_{max}^2}$$

The value of the equivalent Von Mises stress is 318.2MPa , well below the yielding stress of the material of which the pin is composed.

4.3.2 Bearing Verification

Having the reacting forces, it is possible to choose the model of the bearings. The load on these supports is pretty high and the space on the chassis is limited. For this reason, it has been chosen needle roller bearings, that allow high load with a thin thickness.

The bearings need to support, respectively :

- 4140 N;
- 3000 N

CHAPTER 4. TRANSMISSION

From the SKF catalogue, it is found the following model: SKF K15x19x17.

Dimensions	Performance
Bore diameter of needle roller complement	15 mm
Outside diameter	19 mm
Outside diameter of needle roller complement	19 mm
Width	17 mm
	Basic dynamic load rating
	10.8 kN
	Basic static load rating
	15.6 kN
	Limiting speed
	28 000 r/min
	Reference speed
	24 000 r/min

Figure 4.10: Data Sheet of SKF K15x19x17

As shown in 4.10, the static allowable load is 15.6 KN which is 3.8 times larger than the max force on it, and as in the system the load is mainly static because the box has only little rotation around the pin axis, the bearings are verified.

Chapter 5

Box

To contain the transmission gears and to allow the rotation of the blades, but at the same time guarantee the possibility of transmitting the force from one blade to the other, a box is required.

5.1 Parameters

The box must:

- Housing the two bases of the blades and the transmission gears;
- Allowing the rotation of the blades;
- Resist to the forces transmitted from the blades to the box;
- Be the smallest possible;
- Be the lighter possible;
- Respect the overall dimensions;
- Simple to machine;
- Easy to assemble/disassemble;
- Isolated to external agents;

After defining the transmission method and after sizing the gears, were known the broad dimensions and geometry that the box must have.

5.2 Concepts

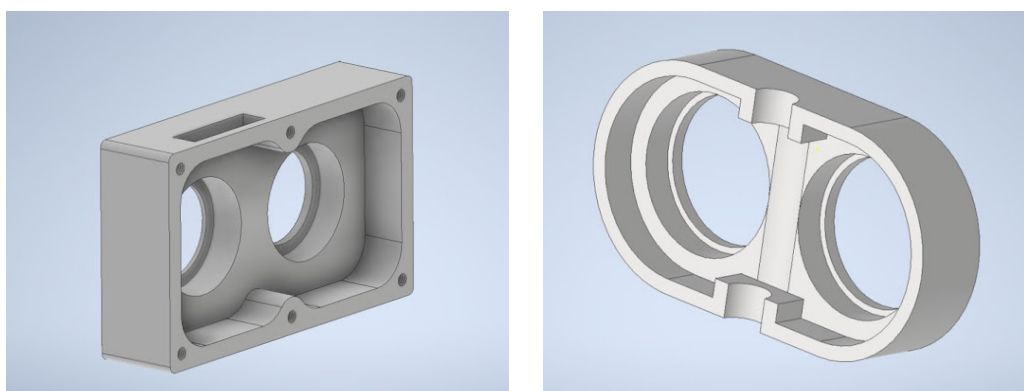


Figure 5.1: First and second concepts: a)based on bevel gears b)based on the worm drive method

Initially, two types of cases were evaluated as the method with which to adjust the inclination of the blades had not yet been precisely decided. The possible concepts generated are therefore those that can be seen in figure 5.1. The first concept exploits the adjustment of the inclination of the blades through a system of cogwheels all connected to each other. This box consists of two parts: one contains all the wheels, while the other acts as a lid. The whole thing is tightened with a few screws. This concept has the advantage that it can be narrow, but at the same time, it needs a large width due to the larger sprockets. Also, to transfer the mode from the motor to the blades, there is an additional sprocket placed halfway out of the box. This solution does not make the box very hermetic and increases the final height of the mechanism. The second concept, on the other hand, immediately had more confidence. It is made up of two symmetrical parts joined together by means of some screws. The concept thus developed is more evolved than the previous one and it uses the worm drive method to transmit the motion to the blades. What was obtained is a concept that has smaller dimensions than the previous and it is entirely symmetrical.

Subsequently, seeing that the transmission system with worm drive was more performing and better in terms of size, more focus were imposed on the development of more optimized and lighter boxes concepts. What it was developed were therefore the models shown in the figure 5.2:

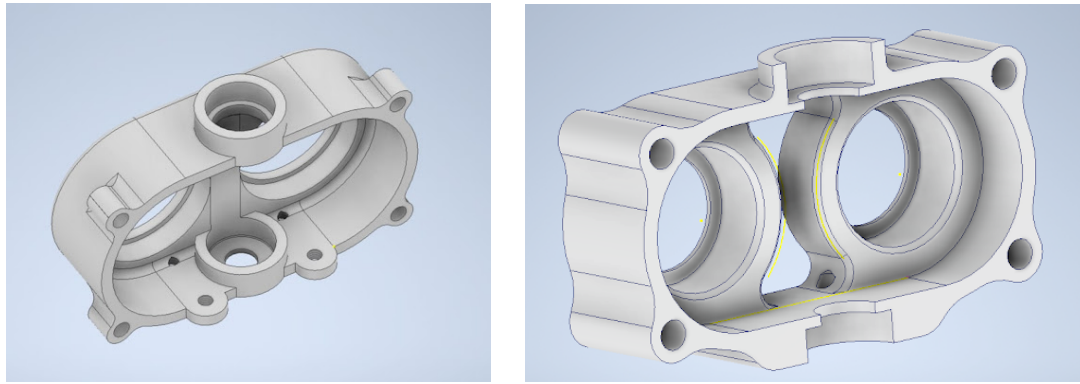


Figure 5.2: Final concepts based on the worm drive method

The concept on the left is an evolution of the one in figure 5.1b, in which have been added the bearing housings and the screw structures to allow closure with a cover. From this, further improvement has been done starting to create an optimized, more symmetrical and lighter box. The final result is a box formed by two perfectly symmetrical pieces, with the absence of material between the holes of the two blades for loosening weight. In addition, the holes for tightening have been integrated into the structure to optimize space and finally, the shape has been optimized to be as small as possible.

5.2.1 Decision matrix

To decide which was the most promising concept, a decision matrix was compiled among the 4 concepts previously seen based on the main characteristics (to which weights were given to evaluate their importance).

Box Specifications	Weight Parameter	Concept 1			Concept 2			Concept 3			Concept 4		
		Mag	Score	Value									
Main dimension	0,30 mm	149	3	0,9	99,3	8	2,4	99,3	8	2,4	87	10	3
Easy to manufacture	0,30 Ranking	Great	10	3	Fair	4	1,2	Great	9	2,7	Great	9	2,7
Easy to assemble/dissassemble	0,10 Ranking	Good	8	0,8	Ok	6	0,6	Good	8	0,8	Good	8	0,8
Good looking	0,05 Ranking	Fair	4	0,2	Good	8	0,4	Good	8	0,4	Good	9	0,45
Weight	0,05 g	945	3	0,15	183	8	0,4	182	8	0,4	196	7	0,35
Isolation from external agents	0,20 Ranking	Poor	2	0,4	Okay	6	1,2	Okay	6	1,2	Okay	6	1,2
Overall Value		5,45			6,20			7,90			8,50		

Figure 5.3: Box decision matrix among the 4 concepts previously presented

From the decision Matrix, it appears that the last optimized concept is the most promising one, consequently, the study has been entirely developed on it.

5.3 Components

The complete box is made up of two main elements:

- the two symmetrical halves;
- the elements that allow them to be assembled.

5.3.1 Verification

Box

From the analysis of the blades, it comes out that the forces applied on the bushing housings from the two blades are:

- $R_a = 2360 \text{ N}$;
- $R_b = 2951 \text{ N}$.

Where R_a is the force applied on the first housing and R_b is the force applied on the other one. The forces have the same direction and are tilted by the same angle as the forces acting on the blades.

Importing the Inventor model of the box in Ansys for the FEM analysis and adding the forces applied by the blades to the bushing housing, it was possible to view the stresses inside the structure, as can be seen in the figure 5.4.

From the analysis, the spots on the mesh that become yellow/red are the points in the box with higher stresses. On the most critical point, it is obtained a stress that reaches 314.4 MPa (with Von Mises method), but that's not a realistic behavior because, due to how the FEM analysis works, in those points the mesh density is much higher, and in consequence, the stresses are higher too.

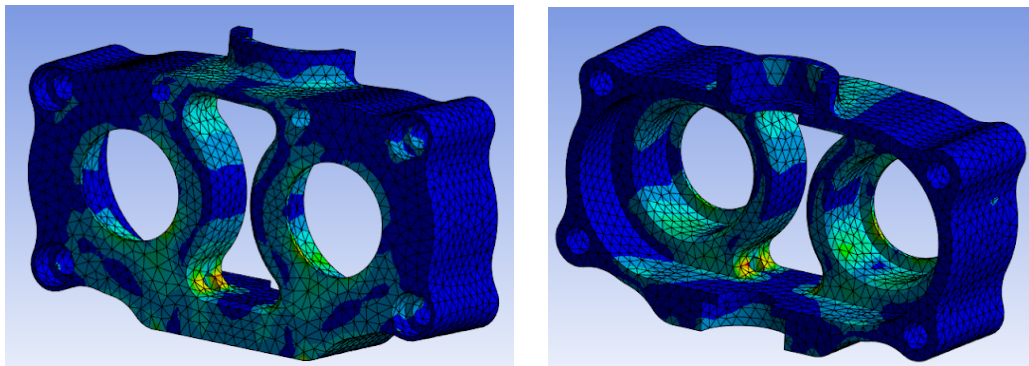


Figure 5.4: Fem analysis of the two halves of the box

Even if the analysis is not realistic, the model obtained represents a worse situation than the real one, consequently, the values obtained are higher than those that the structure actually has to withstand. Checking the box with a material that supports the values obtained with this analysis automatically allows you to check the normal working conditions which represent a more conservative situation.

For the stress values obtained, the structure would be verified using an aluminium alloy as material (figure 5.5) which has a yield strength greater than the maximum load found with the FEM analysis.

Alloy	Temper	Proof Stress 0.20% (MPa)	Tensile Strength (MPa)	Shear Strength (MPa)	Elongation A5 (%)	Elongation A50 (%)	Hardness Brinell HB	Hardness Vickers HV	Fatigue Endur. Limit (MPa)
AA1050A	H2	85	100	60	12		30	30	
	H4	105	115	70	10	9	35	36	70
	H6	120	130	80	7		39		
	H8	140	150	85	6	5	43	44	100
	H9	170	180			3	48	51	
	O	35	80	50	42	38	21	20	50
AA2011	T3	290	365	220	15	15	95	100	250
	T4	270	350	210	18	18	90	95	250
	T6	300	395	235	12	12	110	115	250
	T8	315	420	250	13	12	115	120	250
	H2	115	135	80	11	11	40	40	
AA3103	H4	140	155	90	9	9	45	46	130
	H6	160	175	100	8	6	50	50	
	H8	180	200	110	6	6	55	55	150
	H9	210	240	125	4	3	65	70	
AA5083	O	45	105	70	29	25	29	29	100
	H2	240	330	185	17	16	90	95	280
	H4	275	360	200	16	14	100	105	280
	H6	305	380	210	10	9	105	110	
	H8	335	400	220	9	8	110	115	
AA5251	H9	370	420	230	5	5	115	120	
	O	145	300	175	23	22	70	75	250
	H2	165	210	125	14	14	60	65	
	H4	190	230	135	13	12	65	70	230
	H6	215	255	145	9	8	70	75	
AA5754	H8	240	280	155	8	7	80	80	250
	H9	270	310	165	5	4	90	90	
	O	80	180	115	26	25	45	46	200
	H2	185	245	150	15	14	70	75	
	H4	215	270	160	14	12	75	80	250
AA6063	H6	245	290	170	10	9	80	85	
	H8	270	315	180	9	8	90	90	280
	H9	300	340	190	5	4	95	100	
	O	100	215	140	25	24	55	55	220
	O	50	100	70	27	26	25	85	110
AA6082	T1	90	150	95	26	24	45	45	150
	T4	90	160	110	21	21	50	50	150
	T5	175	215	135	14	13	60	65	150
	T6	210	245	150	14	12	75	80	150
	T8	240	260	155		9	80	85	
AA6262	O	60	130	85	27	26	35	35	120
	T1	170	260	155	24	24	70	75	200
	T4	170	260	170	19	19	70	75	200
	T5	275	325	195	11	11	90	95	210
	T6	310	340	210	11	11	95	100	210
AA7075	T6	240	290		8				
	T9	330	360		3				
	O	105	225	150		17	60	65	230
AA7075	T6	505	570	350	10	10	150	160	300
	T7	435	505	305	13	12	140	150	300

Figure 5.5: Main types of aluminium alloys for the construction of the box. Source: [1]

Box joint

The procedures for checking the box bolted joints are fully analyzed in chapter 7.2 as they are also shared for the other elements.

Chapter 6

Motor

6.1 Motor

No torque is theoretically required to allow the knives to rotate through the torque action of the motor. In practice, however, we know that between the transmission couplings there is friction which means that a minimum of torque is needed to move the elements. For this reason, a motor with a high torque (compared to the necessary one) was chosen, which allows for high control precision, while maintaining small dimensions. A motor that allows these parameters to be respected is the stepper-type motor. The choice was a Nema 17 motor that has:

- Electric specimens:
 - Motor type: bipolar stepper;
 - Angular step: 1,8°;
 - Holding torque: 55 N cm;
 - Nominal current/phase: 2,0 A;
 - Phase resistant: 1,3 ohm;
 - Inductance: 2,4 mH ± 20%.
- Physical specifications
 - Width x length: 42 x 42 mm;
 - Height: 48 mm;
 - Shaft diameter: \varnothing 5mm;
 - Shaft length: 24 mm;
 - D-cut length: 15 mm;
 - Wires number: 4;
 - Wire length: 1000 mm.

6.2 Transmission coupling

To connect the worm gear to the motor, it has been designed two concepts. What we need in this case is to have a flexible joint between the motor shaft and the worm gear. This is because if there is any alignment error between the two axes, with the rigid connection, there is unwanted load both on gear and motor, and it may cause the break of the component.

6.3 Motor support

To allow the assembly of the engine above the transmission, two different paths were chosen:

1. The first was to look for a way that would allow obtaining light and optimized structure based on the forces acting on it;
2. The second, instead, focused on designing and verifying a very simple element as similar as possible to what the market offers (consequently also much cheaper than the first solution).

6.4 Concepts

For the transmission coupling, there were two concepts: the first involves the use of a flexible coupling to connect the motor shaft to that of the worm screw. The second, on the other hand, involves interposing a rubber mat between the motor plate and the support, which, in addition to relaxing the specifications regarding the precision of the coupling, also acts as a vibration damper.

For the engine support, however, the first concept was based on the optimization of a cylindrical element subjected to the twisting action of the engine. The second concept, on the other hand, uses a common L-shaped bracket on which the holes for fixing the complete structure and the engine are made. In addition, other holes have been made in the low-stress areas to make the complete structure lighter.

The 2 final concepts are therefore the union of the 4 in the previous points. The 2 best concepts are, therefore:

1. Optimizes bracket with an elastic joint (a);
2. L-bracket with rubber mat (b) (as can be seen in the figure 6.1).

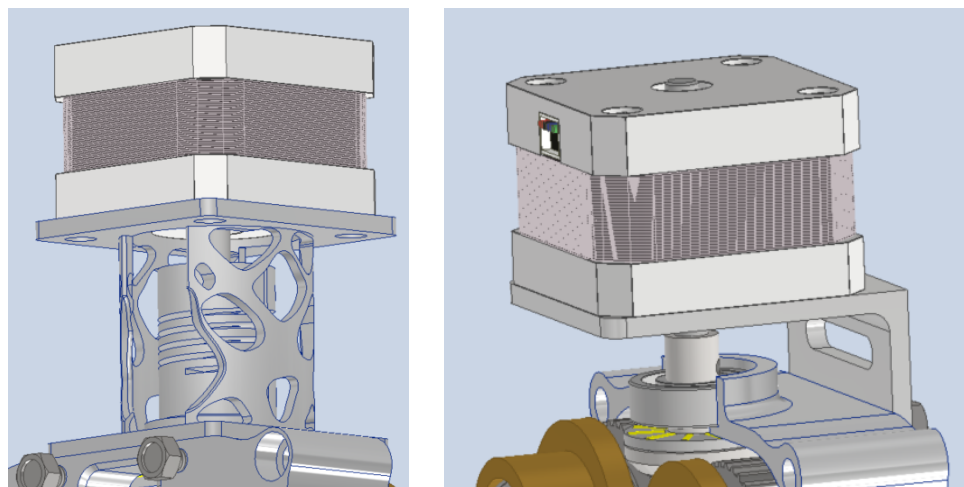


Figure 6.1: Motor support concepts: a) Optimized b) Easier and cheaper

6.4.1 Decision matrix

Motor support			Concept 1			Concept 2		
Specifications	Weight	Parameter	Mag	Score	Value	Mag	Score	Value
Main dimension (height)	0,30 mm		71	5	1,5	48	9	2,7
Easy to manufacture	0,30	Ranking	Great	4	1,2	Fair	10	3
Easy to assemble/dissassemble	0,10	Ranking	Good	8	0,8	Ok	6	0,6
Good looking	0,05	Ranking	Fair	10	0,5	Good	8	0,4
Weight	0,05 g		26	8	0,4	16	9	0,45
Axial compensation	0,20	Ranking	Poor	10	2	Okay	7	1,4
Overall Value					6,4			8,55

Figure 6.2: Motor support and transmission concepts

From the decision matrix, it came out that the second concept is better than the other because it's easier to manufacture and much smaller, so, lighter.

6.5 Verification

Analyzing the forces transmitted by the motor to the support, the forces that the structure must support are:

- Shear Resistance: Negligible;
- Tension Resistance: $\sigma_{min} = 9.43 \text{ MPa}$;
- Punching Resistance: $\sigma_{min} = 1.88 \text{ MPa}$.

Therefore, continuing with the idea of using products already existing on the market and that the finished support is as light as possible, the choice of material with which to make the bracket fell on aluminium which has a yield strength of $\sigma_{uts} = 90 \text{ MPa}$, which verifies the tightness of the structure.

The verification of the tightness of the bolts, on the other hand, is analyzed in a special section (section 7.3), as seen previously for the other elements

Chapter 7

Bolted Joints

7.1 General bolt verification procedure

All the components of the anti-roll bar are connected using a bolted joint connection. To choose the correct material and class of bolts we have done a static verification. Is important to take into account that bolts realize a statically undetermined constraint. So we consider that the bolts have an elastic behavior to accommodate all the deformations. We assume to interface with rigid members and deformable bolts, that are modeled like mono-dimensional elastic elements.

The first step is to find the forces that are transferred by the joint. The loads are studied independently, and then summed together using the superimposition theorem. Once you have found the loads for each bolt, you start verifying the most critical. You have to ensure that both the bolt and the plate will not break.

7.1.1 Different type of load

Shear force

The shear on each bolt will be parallel to the total shear (V) and proportional to bolt stiffness (as shown in figure 7.1).

$$V_i = \frac{V A b_i}{\sum_{i=1}^{N_b} A b_i}$$

Where $A b_i$ is the bolt tensile cross-section and N_b the number of bolts.

If the resisting cross section is equal for each bolt:

$$V_i = \frac{V}{N_b}$$

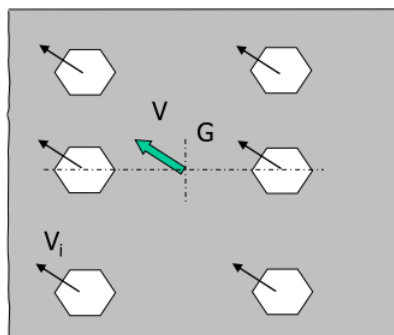


Figure 7.1: Shear on each bolt (V_i).

Torsion

Assume to have a rigid rotation about the centroid (G). The elongation of the bolts is proportional to the distance from the centroid and the resisting area (as shown in figure 7.2).

$$V_i = \frac{T A b_i r_i}{\sum_{i=1}^{N_b} A b_i r_i^2}$$

If the resisting cross section is equal for each bolt:

$$V_i = \frac{T r_i}{\sum_{i=1}^{N_b} r_i^2}$$

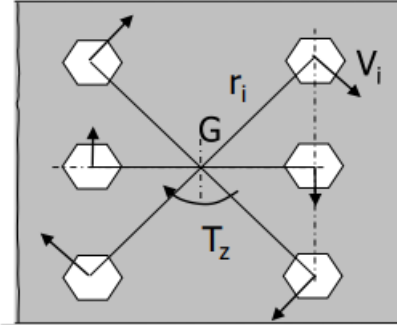


Figure 7.2: Shear on each bolt (V_i).

Normal

The normal load on each bolt will be parallel to the total normal force (N) and proportional to bolt stiffness (as shown in figure 7.3)

$$N_i = \frac{N A b_i}{\sum_{i=1}^{N_b} A b_i}$$

If the resisting cross section is equal for each bolt:

$$N_i = \frac{N}{N_b}$$

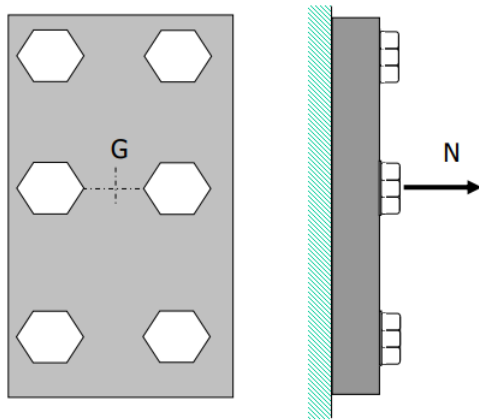


Figure 7.3: Normal on each bolt (N_i).

Bending

To have a more accurate study occur consider the plate as a semi-rigid member. This generates a separation action on the bolts (normal load) and a compressive action that opposes the contact between plates (as shown in figure 7.4). Further hypotheses must be taken into account like plane sections remain plane and linear stress distribution.

$$\sigma = -\sigma_{max,co}(1 - \frac{y}{y_n})$$

$$N_i = \sigma(y_i)Ab_i$$

But in this two relationships are unknown $\sigma_{max,co}$ and y_n , so they should be found with the solution of the system composed by the translation and rotation (about neutral axis y_n) equations.

Translation equation:

$$\int_0^{A(y_n)} \sigma(y) dA + \sum_{i=1}^{N_{bt}} -\sigma_{max,co} \left(1 - \frac{y_i}{y_n}\right) Ab_i = N$$

Rotation equation:

$$\int_0^{A(y_n)} \sigma(y)(y - y_n) dA + \sum_{i=1}^{N_{bt}} -\sigma_{max,co} \left(1 - \frac{y_i}{y_n}\right) (y_i - y_n) Ab_i = M_b + N(y_g - y_n)$$

Where N_{bt} is the number of bolts in tension.

To find y_n you should use an iterative approach. First of all, you guess the number of bolts in tension in order to evaluate y_n from the system. Then you check that the number of bolts in tension is correct.

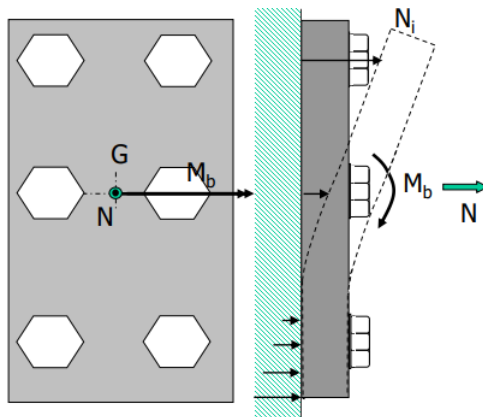


Figure 7.4: Normal on each bolt (N_i).

7.1.2 Different type of verifications

Tension resistance

The tension resistance of bolts is given by:

$$N_b \leq \frac{A_{bt}\sigma_R}{\phi}$$

Where A_{bt} is the bolt tensile cross-section and σ_R the ultimate tensile strength of the bolt. According to Eurocode 3 $\phi = 1.25/0.9$.

Punching resistance

Punching resistance avoids the cut of the member by the head of the bolt.

$$N_b \leq \frac{\pi d_0 t \sigma_{R,m}}{\phi}$$

Where d_0 is the bolt head diameter, t the thickness of the plate and $\sigma_{R,m}$ the ultimate tensile strength of the plate.

According to Eurocode 3 $\phi = 1.25/0.6$.

Shear resistance

The shear resistance of bolts is given by:

$$V_b \leq \frac{A_b \sigma_R}{\phi}$$

Where A_b is the bolt cross-section subject to shear.

According to Eurocode 3 $\phi = 1.25/0.9$.

Crushing resistance

The crushing resistance of members is given by:

$$V_b \leq \frac{dt \sigma_{R,m}}{\phi}$$

Where d is the bolt diameter.

According to Eurocode 3 $\phi = 0.5$.

Sliding resistance

The sliding resistance of a preloaded bolt avoids the sliding of the plates subject to shear.

$$V_b \leq \frac{k_s n f}{\phi} (N_0 - 0.8 N_b)$$

Where k_s is a coefficient depending on the type of hole (ordinary =1, oversized = 0.85), n is the number of surface pairs in contact, f is the friction coefficient, N_b is the tension actions applied on the bolt and N_0 is the preload of the bolt (equal to the 80% of the yield strength of the bolt).

According to Eurocode 3 $\phi = [1.1, 1.25]$.

7.2 Bolts of the box verification

In order to study the behavior of the bolts that connect the two parts of the box is important to define the loads that the box must carry. The most critical case is when the bearings have to react to the maximum forces that are applied to the blades. These reacting forces are supported by the box and they can be visualized in figure 7.5.

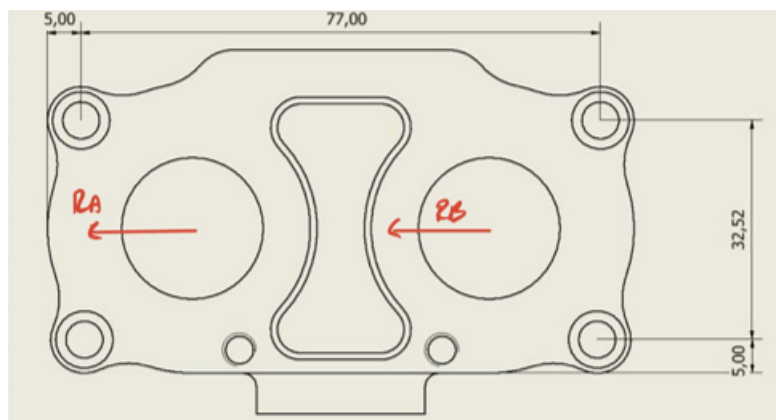


Figure 7.5: Forces applied to the box.

The particular shape of the box was simplified assuming a simpler shape of a rectangle. From the figure, you can see that the loads that the bolts have to carry are shear (resulting from the summation of R_A and R_B) and bending moment (obtained by the product of the resulting force and half thickness of the box). In order to have a good connection and to not increase too much the dimension of the box, it was chosen to use M5x0.5 for all the bolts.

Data of the forces and resulting bending moment:

$$\begin{aligned} R_a &= 2360 \text{ N;} \\ R_b &= 2951 \text{ N;} \\ M_b &= 116842 \text{ Nmm;} \end{aligned}$$

From the study of the verification was obtained the following results:

- Bolt:
 - Shear resistance: $V_b = 2655.5 \text{ N}$ that corresponds to $\sigma_{R,min} = 389.6 \text{ MPa}$;
 - Tensile resistance: $N_b = 1622.6 \text{ N}$ that corresponds to $\sigma_{R,min} = 158.7 \text{ MPa}$;
- Member:
 - Crushing resistance: $\sigma_{R,memb,min} = 14.43 \text{ MPa}$;
 - Punching resistance: $\sigma_{R,memb,min} = 6.68 \text{ MPa}$;
- Sliding resistance:
 - Considering sliding between aluminum surfaces ($f = 1.1$) and a hole coefficient equal to 1, the safety factor results $\phi = 2.47$;

In order to respect the condition on the ultimate tensile strength was chosen the 8.8 class for bolts. This choice was also done considering the easy availability of the type of bolts. For the members there are no problems, so it verified the choice of aluminum.

7.3 Bolts of the motor support verification

The support of the motor is subject to the weight and the torque of the electric motor. Taking into account that the weight is equal to 0.3 Kg, it was considered negligible. So the only load that the bolts must carry is the bending moment generated by the torque of the motor. Also in this case the shape of the member was simplified as can be seen in figure 7.6. The screws chosen are M4x0.5.

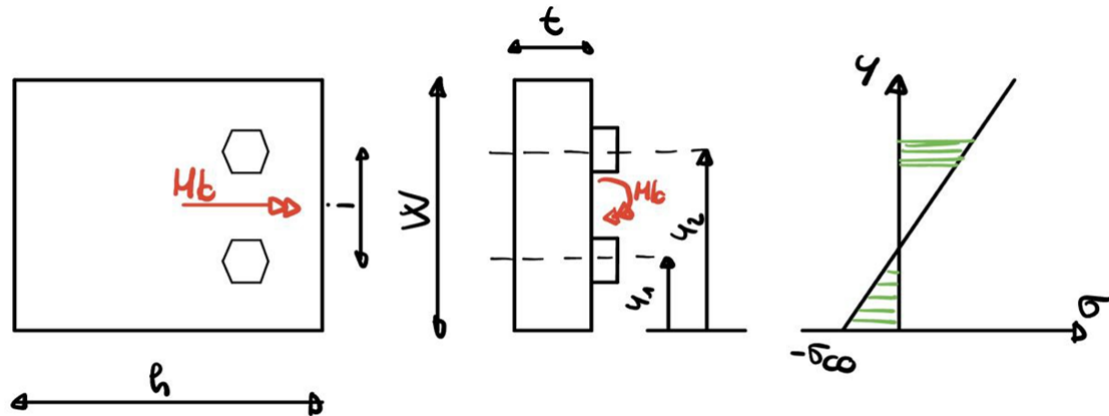


Figure 7.6: Bending moment applied to the support of the motor.

The dimensions of the simplified motor support are the following:

$$h = 27.5 \text{ mm}; \quad i = 30 \text{ mm}; \quad t = 3 \text{ mm}; \quad w = 42 \text{ mm}; \quad y_1 = (w - i)/2; \quad y_2 = y_1 + i;$$

Data of the bending moment:

$$M_b = 2000 \text{ N mm};$$

From the study of the verification was obtained the following results:

- Bolt:
 - Tensile resistance: $N_b = 59.58 \text{ N}$ that corresponds to $\sigma_{R,min} = 9.42 \text{ MPa}$;
- Member:
 - Punching resistance: $\sigma_{R,memb,min} = 1.88 \text{ MPa}$;

The minimum ultimate tensile strength that results from the verification is very low, so we have chosen class 8.8 because it is the mostly used. For the members there are no problems, so it verified the choice of aluminum.

7.4 Bolts of the box-pin plate verification

The connection between the pin support and the box is done by a bolted joint. The bolts must resist to the forces applied to the blades and the resulting bending moment generated by the product of these forces and the distance between the application point and the joint centroid. Verification is done considering the most critical condition. It is possible to see the disposition on the plate of the 4 M4x0.5 bolts in figure 7.7.

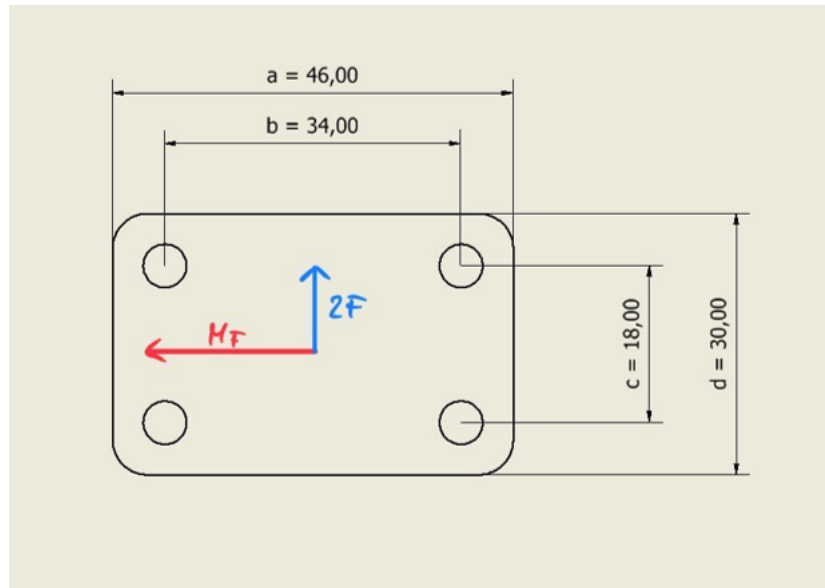


Figure 7.7: Forces applied to the box-pin plate.

Data of the force and the resulting bending moment:

$$F = 591 \text{ N}; \quad M_f = 40779 \text{ N mm};$$

From the study of the verification was obtained the following results:

- Bolt:
 - Shear resistance: $V_b = 295.5 \text{ N}$ that corresponds to $\sigma_{R,min} = 70.12 \text{ MPa}$;
 - Tensile resistance: $N_b = 883.2 \text{ N}$ that corresponds to $\sigma_{R,min} = 139.7 \text{ MPa}$;
- Member:
 - Crushing resistance: $\sigma_{R,memb,min} = 6.16 \text{ MPa}$;

- Punching resistance: $\sigma_{R,memb,min} = 13.9 \text{ MPa}$;
- Sliding resistance:
 - Considering sliding between aluminum surfaces ($f = 1.1$) and a hole coefficient equal to 1, the safety factor results $\phi = 14.1$;

The class of the bolts chosen is 8.8, the way to select it is the same used in the bolted joint of the motor support. For the members there are no problems, so it verified the choice of aluminum.

Conclusions

In conclusion, with all the concepts chosen, the Anti-Roll bar seems to don't have any problems. The design respects all the requirements, it's smaller than what was previously asserted as the space occupied by the system.

All the verifications have been done with an honest amount of safety factor and all the pieces of the Anti-Roll bar support excellently the loads to which they are subjected.

Anyway, there are still some points of the discussion which have not been touched on or which could be made more precisely.

For example, an interesting deepening in our analysis could be about the frequency response of our system, even if it could be very difficult to calculate precisely the frequency of the force to which the blades are subjected. In fact, the oscillations of the track are basically random and of negligible amplitude.

In conclusion, our report touches all the most important and critical points of the design of this innovative Anti-Roll bar, for which the phase of prototyping could start soon.

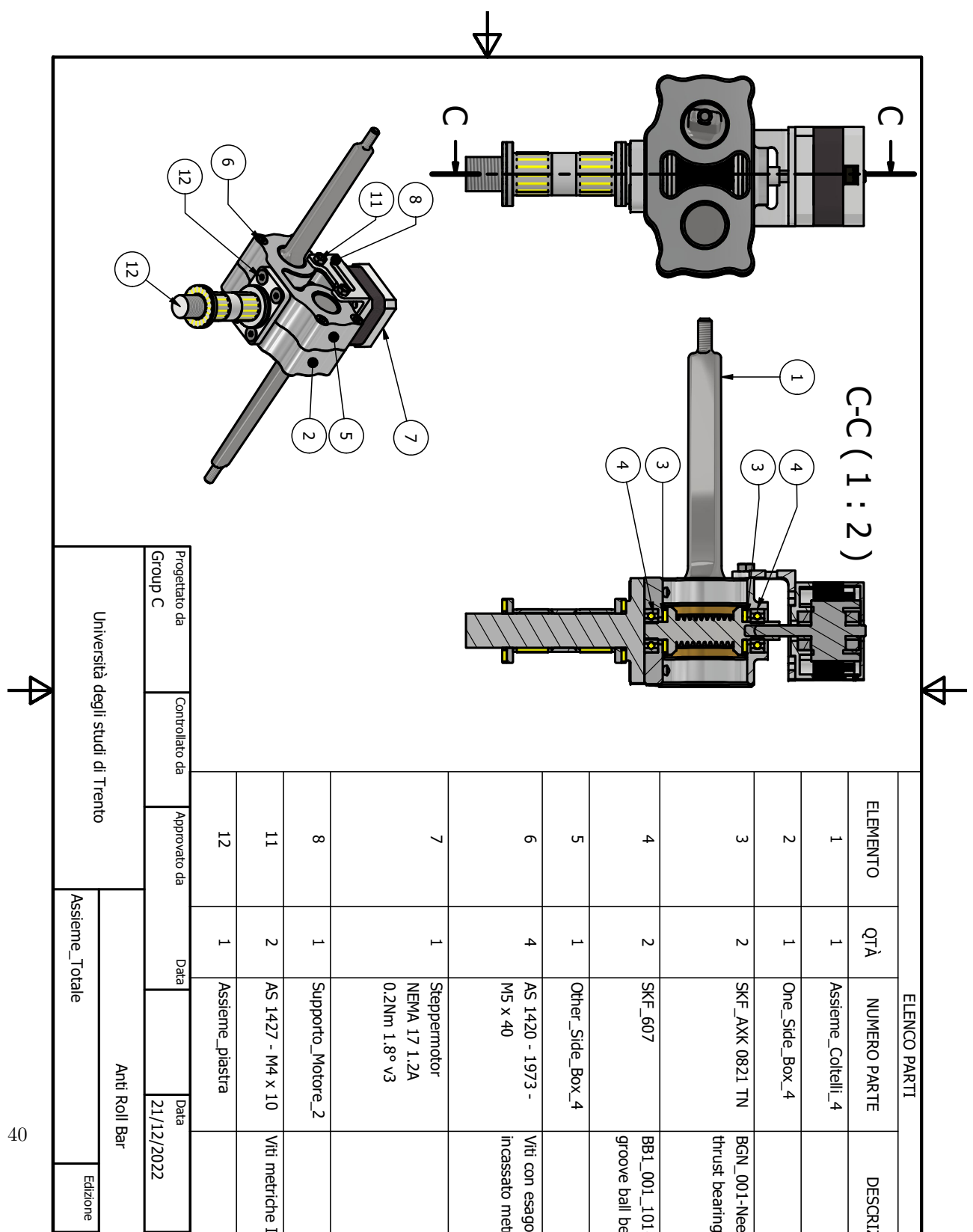
CONCLUSIONS

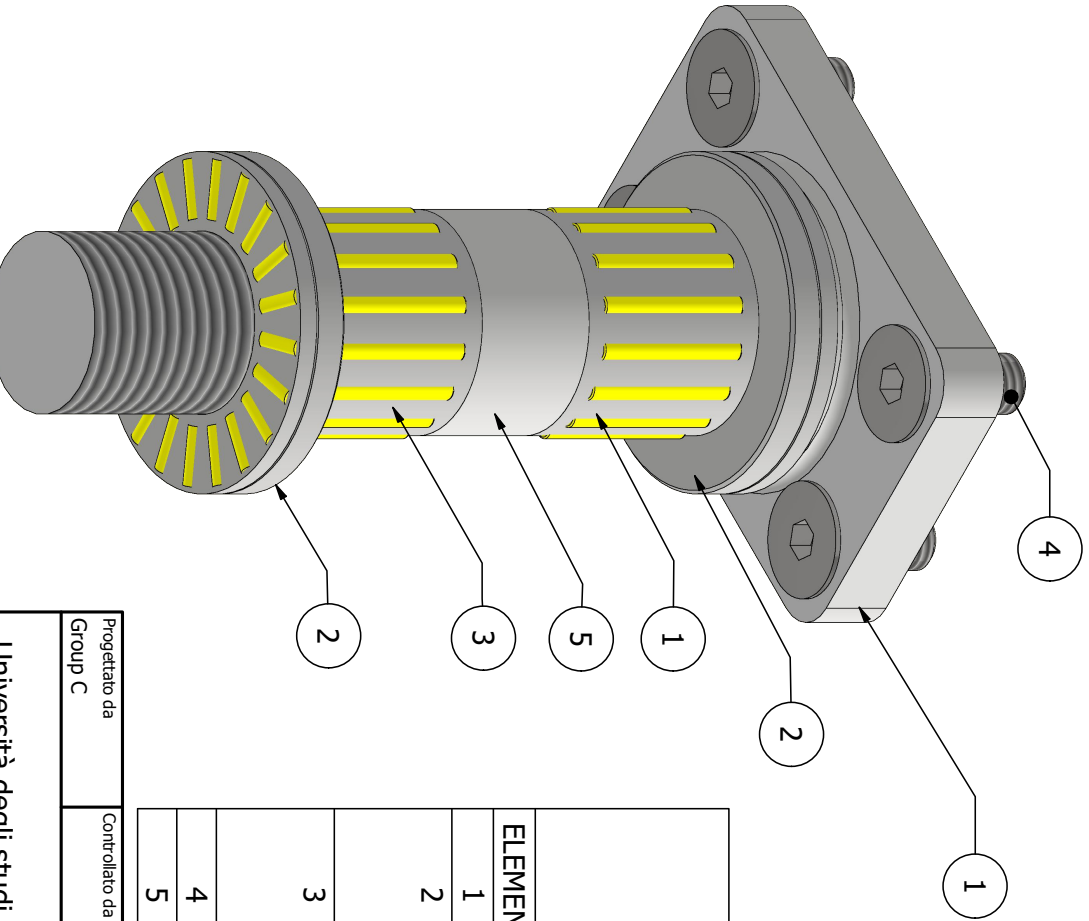
List of Figures

1.1	A consequence of the anti-roll bar removing	1
1.2	The inertia effect on the vehicle's suspensions during a turn, with or without an anti-roll bar	1
1.3	Adjustable roll-bar system, by changing the length of the cantilever	2
1.4	Bladed anti-roll bar	3
1.5	Maximum overall dimensions of the active anti-roll bar	4
1.6	Table of specifications	4
2.1	Final concept of the total system of active anti-roll bar	5
3.1	Blades' model	7
3.2	Internal forces applied on the blade for different angles of rotation	9
3.3	Moments applied on the blade for different angles of rotation	9
3.4	Internal stress of the blade for different angles of rotation	10
3.5	Internal stress of the blade in 3D. $b_0=15$, $h_0=20$, $k=0.07$	10
3.6	Blades decision matrix, for the shape choice	11
3.7	Data Sheet of SKF PBMF 202615M1G	12
4.1	a) First concept b) Second concept	13
4.2	Data sheet of worm gear	14
4.3	Data Sheet of allowable Load on worm gear	14
4.4	Bearings used to support the worm gear	15
4.5	Data Sheet of SKF AXK 0821 TN	15
4.6	3d Model and scheme of the pin	16
4.7	Model of the pin	16
4.8	Plot of M_y and T_x	17
4.9	Plot of σ_{zz}	17
4.10	Data Sheet of SKF K15x19x17	18
5.1	First and second concepts: a)based on bevel gears b)based on the worm drive method	19
5.2	Final concepts based on the worm drive method	20
5.3	Box decision matrix among the 4 concepts previously presented	20
5.4	Fem analysis of the two halves of the box	21
5.5	Main types of aluminium alloys for the construction of the box. Source: [1]	22
6.1	Motor support concepts: a) Optimized b) Easier and cheaper	24
6.2	Motor support and transmission concepts	24
7.1	Shear on each bolt (V_i).	27
7.2	Shear on each bolt (V_i).	28
7.3	Normal on each bolt (N_i).	28
7.4	Normal on each bolt (N_i).	29
7.5	Forces applied to the box.	30
7.6	Bending moment applied to the support of the motor.	31
7.7	Forces applied to the box-pin plate.	32

LIST OF FIGURES

Technical Drawings





ELENCO PARTI

ELEMENTO	QTÀ	NUMERO PARTE	DESCRIZIONE
1	1	Piatra	
2	2	SKF_AXK 1528 + LS 1528-rcw	BGN_001-Needle roller thrust bearings
3	2	SKF_K 15X19X17	BN1_001-Needle roller and cage assemblies
4	4	UNI 5933 - M5 x 12	Vite svasata
5	1	Boccola piastra	

Progettato da
Group C

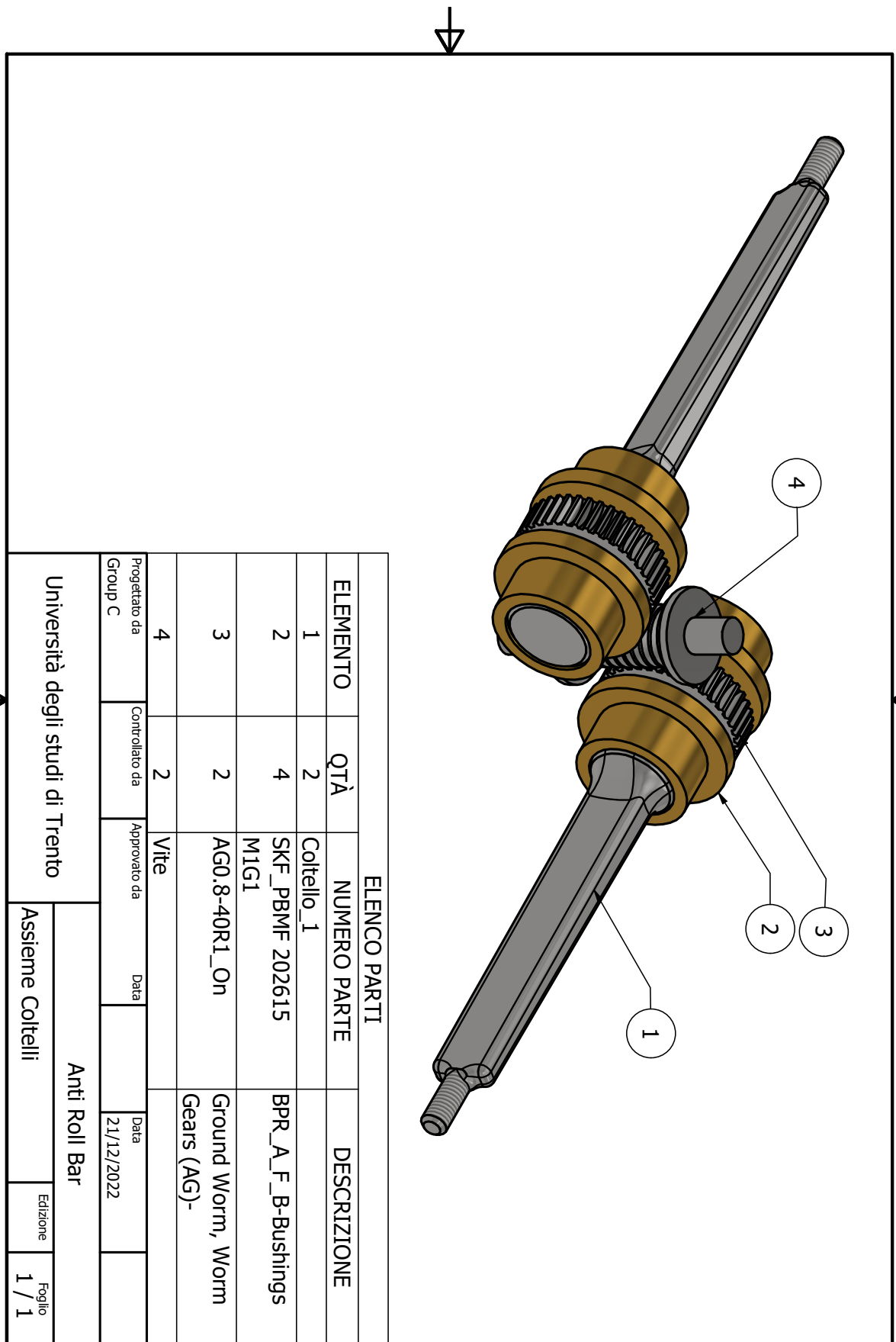
Controllato da
Approvato da
Data

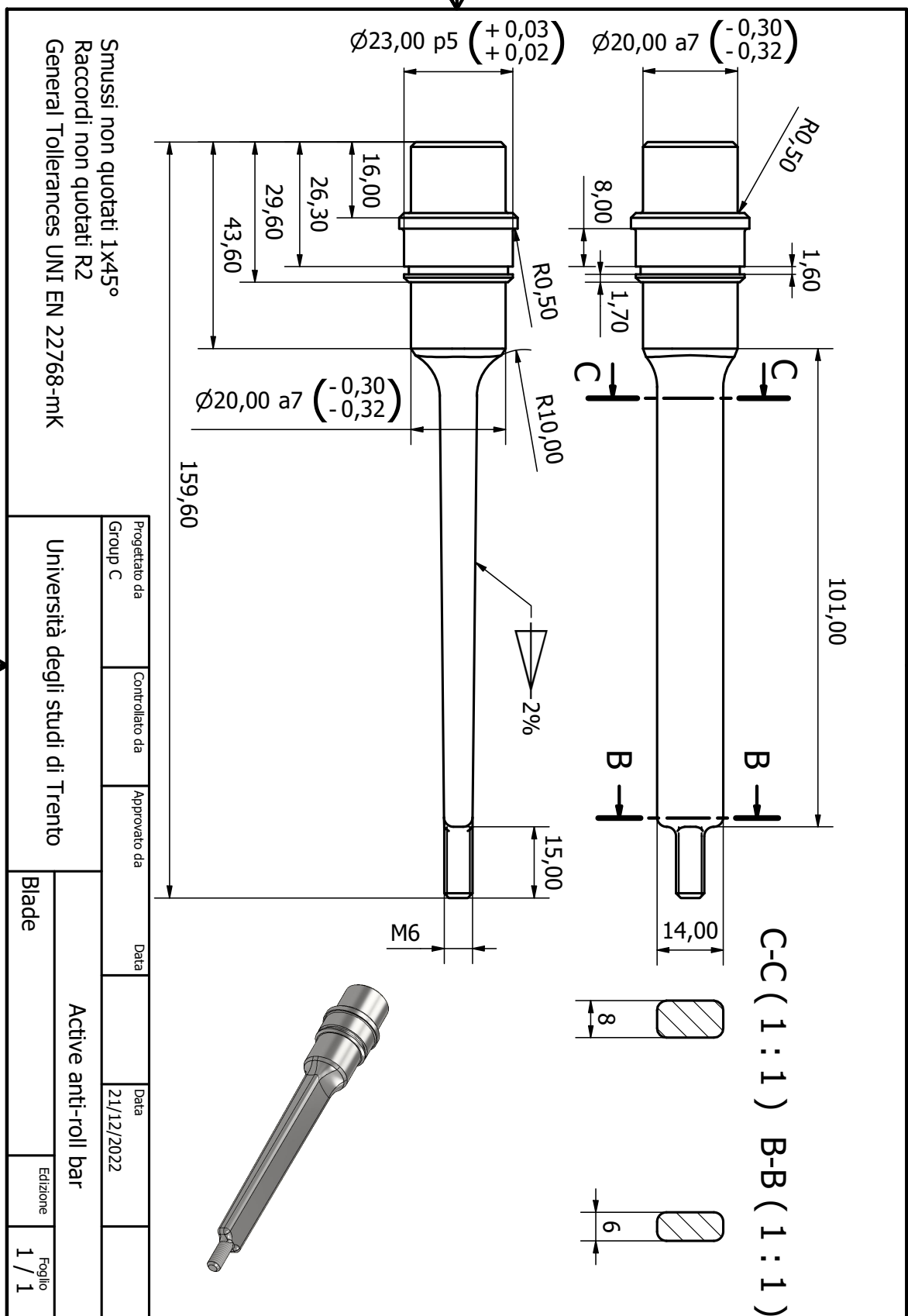
Data

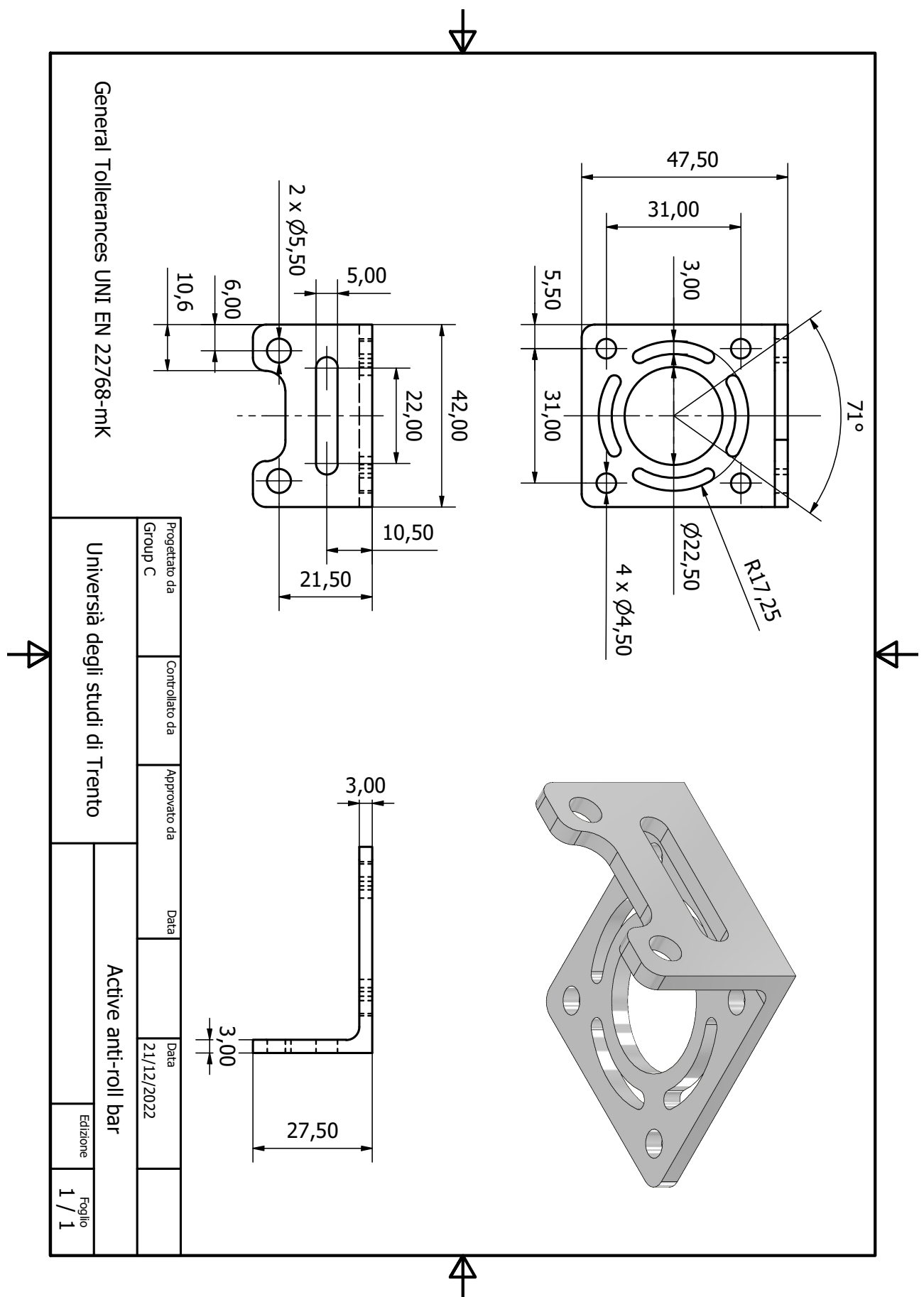
21/12/2022

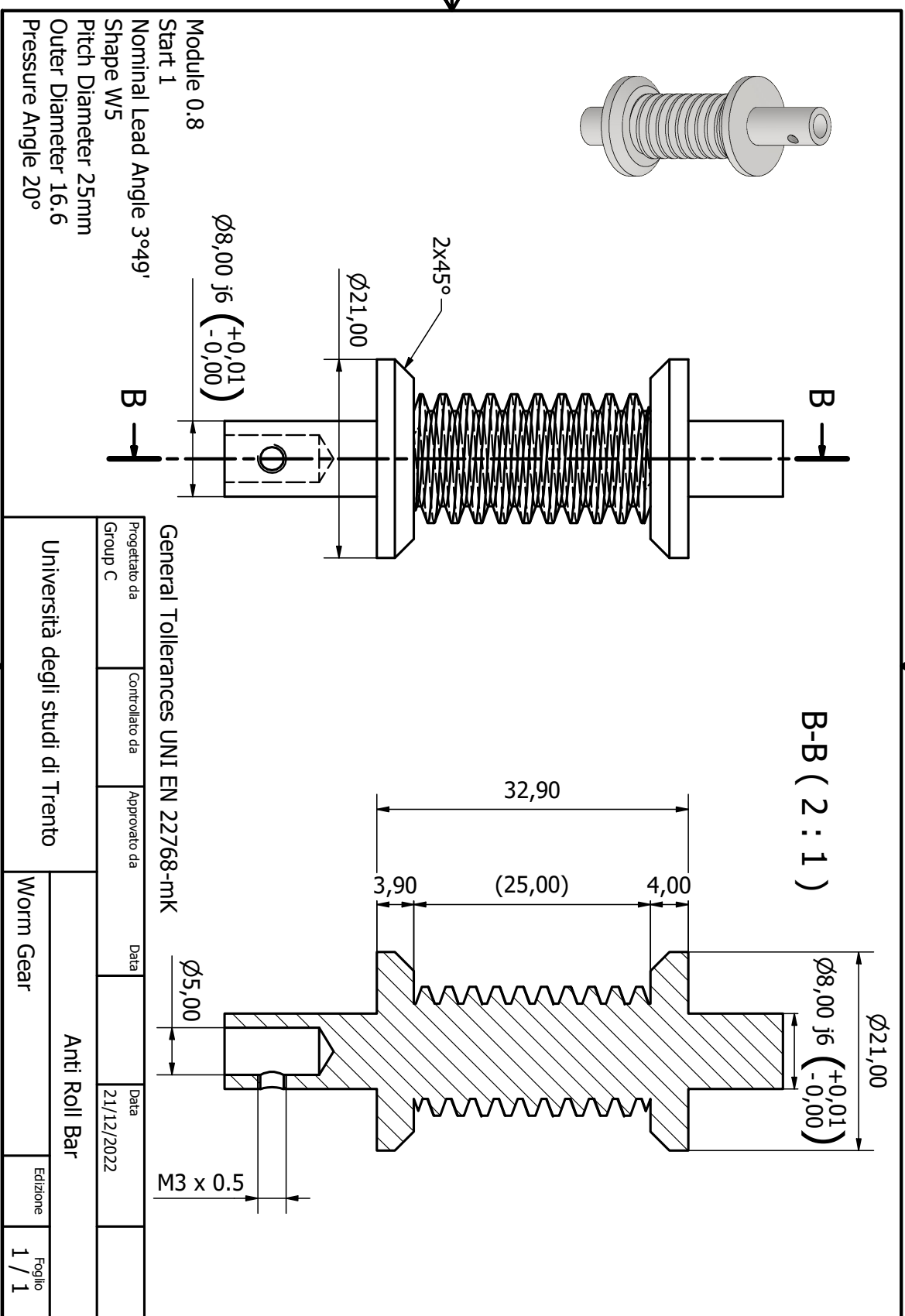
Università degli studi di Trento

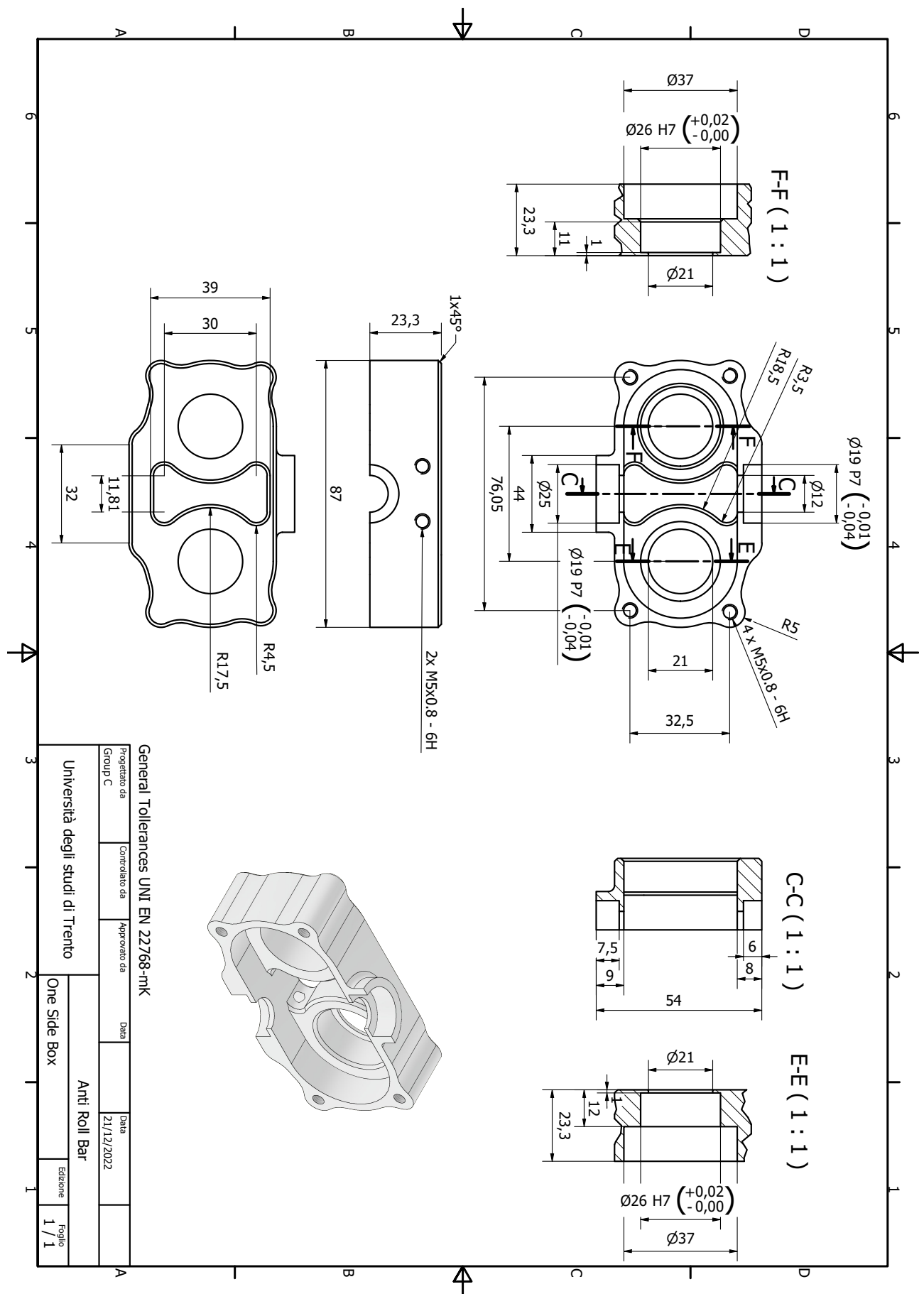
Anti Roll Bar
Assieme Piatra
Edizione
1 / 1

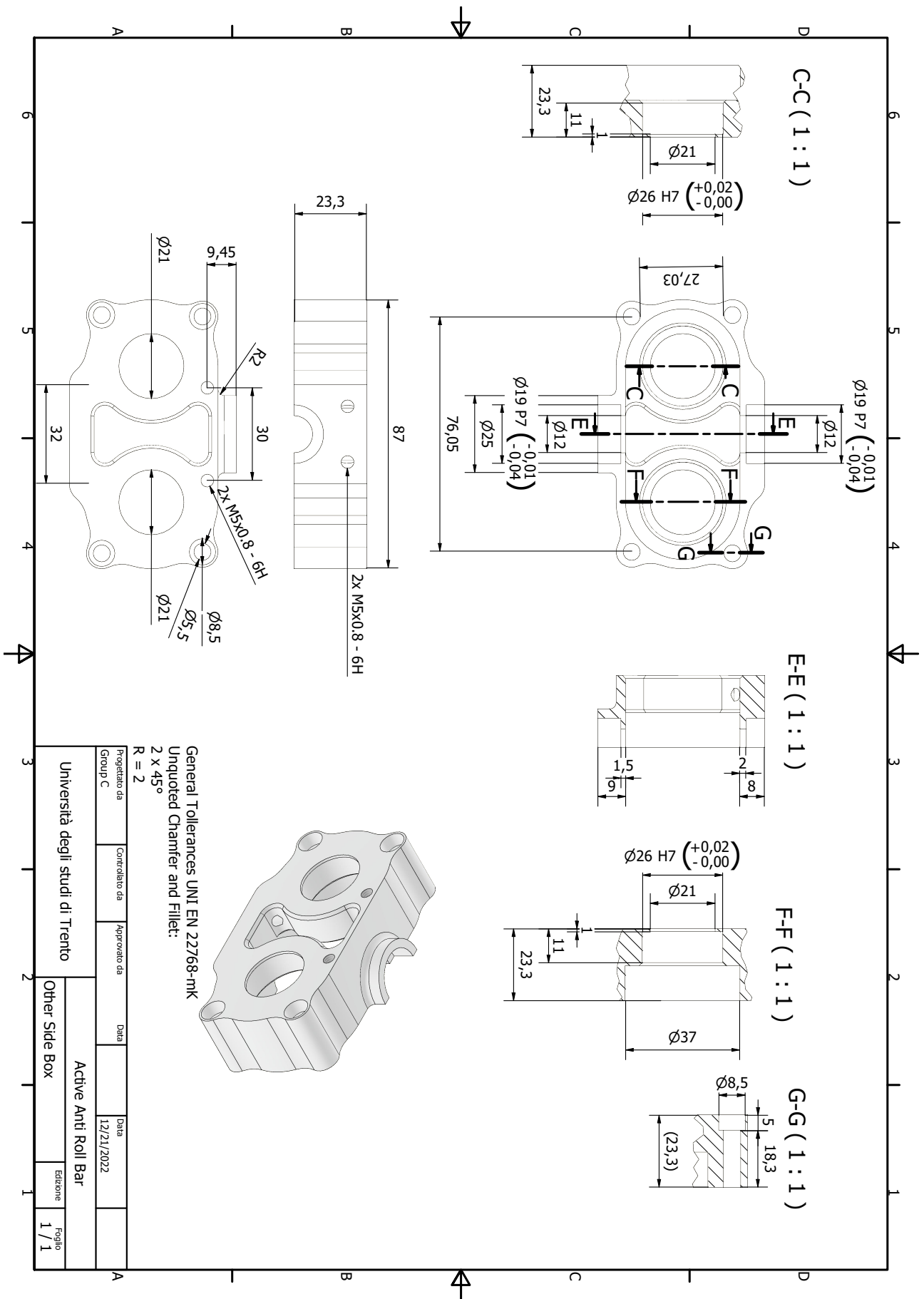












CHAPTER 7. TECHNICAL DRAWINGS

Gear Type	Worm Gears	Construction	Ground Worm Shafts
Nominal Axial Module	0.8	Number of Start	1
Nominal Lead Angle	3°49'	Hand of Thread	Right Hand
Shape	W5	Shaft Diameter / Bore (A)	8.0 (mm)
Shaft Length Left (F)	25.0 (mm)	Pitch Diameter (P)	12.0 (mm)
Outer Diameter (Q)	13.6 (mm)	Face Width (M)	20.00 (mm)
Shaft Length Right (F)	40.0 (mm)	Total Length (J)	85.00 (mm)
Weight	0.04300 (kg)	Precision Grade	KHK W 001 grade 2
Reference Section of Gear	Axial	Gear Teeth Type	Standard Full Depth
Pressure Angle	20°	Material	SCM440 (AISI 4140) Alloy Steel
Heat Treatment	Thermal Refined, tooth surface Induction Hardened	Tooth Hardness	HRC 50-60